BAND STRUCTURE AND TRANSPORT PROPERTIES OF SIMPLE CUBIC TELLURIUM-BASE ALLOYS

Thesis by

Lawrence R. Newkirk

In Partial Fulfillment of the Requirements

For the Degree of

Doctor of Philosophy

California Institute of Technology

Pasadena, California

1970

(Submitted March 4, 1970)

To my wife and parents

ACKNOWLEDGEMENT

The author wishes to express his deepest gratitude to Professor Pol Duwez and Dr. C. C. Tsuei for the help and encouragement extended throughout this work. Technical assistance from J.E. Brown, C. Geremia, S. Kotake, P.K. Kuan, R. Sacks, J.A. Wysocki, and F. Youngkin is also gratefully acknowledged.

This work was made possible by grants from the United States Atomic Energy Commission.

The author also wishes to express his sincere gratitude to his wife Cheri for her encouragement and tolerance during the course of this work.

ABSTRACT

The electrical transport properties and lattice spacings of simple cubic Te-Au, Te-Au-Fe, and Te-Au-Mn alloys, prepared by rapid quenching from the liquid state, have been measured and correlated with a proposed band structure. The variations of superconducting transition temperature, absolute thermoelectric power, and lattice spacing with Te concentration all showed related anomalies in the binary Te-Au alloys. The unusual behavior of these properties has been interpreted by using nearly free electron theory to predict the effect of the second Brillouin zone boundary on the area of the Fermi surface, and the electronic density of states. The behavior of the superconducting transition temperature and the lattice parameter as Fe and Mn are added further supports the proposed interpretation as well as providing information on the existence of localized magnetic states in the ternary alloys. In addition, it was found that a very distinct band structure effect on the transition temperatures of the Te-Au-Fe alloys could be identified.

TABLE OF CONTENTS

I. INTRODUCTION

Among the elements, only Polonium has the simple cubic crystal structure with one atom per unit cell[1]. This type of structure has not been found in equilibrium alloys, but several metastable phases, obtained by rapid cooling from the liquid state, have been reported[2-4]. Among these are Te-Au alloys containing 55-85 at% Te[2]. In the present investigation, measurements of the lattice spacing, thermoelectric power, and superconducting transition temperature of Te-Au alloys are reported. In addition, the effects of a small amount of Fe or Mn on the lattice parameter, the superconducting transition temperature and the magnetoresistance of the simple cubic Te-Au alloys are studied.

The simple cubic crystal structure is well suited for the study of Fermi surface-Brillouin zone interactions because the Brillouin zone construction is rather straightforward and relatively easy to visualize. In addition, the topology of the Fermi surface is anticipated to be rather simple. The usual methods for studying the topology of the Fermi surface, such as magnetoresistance, acoustic resonance, cyclotron resonance, etc., have very important drawbacks. These methods require a long electron mean free path, and a knowledge of crystal orientation. In the case of an element both of these criteria can be satisfied by the use of a single crystal. The high degree of perfection leads to a long electron mean free path, and the knowledge of the crystal orientation allows one to fix directions in reciprocal space. In the case of alloys, however, the problem becomes considerably more difficult. The addition of small amounts of alloying

elements substantially reduces the electron mean free path causing the measurements to become more difficult to interpret. Furthermore, in the case of metastable alloys the conventionally used techniques fail completely since one usually is limited to the use of polycrystalline specimens, frequently with a very small grain size. In the present investigation it is shown that much may be learned about the topology of the Fermi surface and about its interaction with the Brillouin zones through the study of ordinary transport properties in the polycrystalline material. An attempt is made to show how the interpretation of lattice spacings, superconducting transition temperature, thermoelectric power, and magnetoresistance measurements of the systems Te-Au and Te-Au-Fe can lead to an understanding of the nature of the Fermi surface-Brillouin zone interaction.

II. EXPERIMENTAL PROCEDURES

A. Preparation of Alloys

All the alloys used in this study were prepared by induction melting of appropriate amounts of the constituents listed in Table I. The materials for each alloy were placed in a fused quartz crucible, evacuated, flushed with argon, re-evacuated and refilled to atmospheric pressure with argon (99.99% purity), then melted at $\sim 800^{\circ}C$ in an induction furnace. After final weighing, the alloys were drawn into one and two mm. rods using quartz tubing. The weight loss following melting was less than 0.2% so the nominal alloy compositions were taken as the actual ones.

B. Quenching Technique

The simple cubic phase was obtained by quenching a small amount of alloy ($\sim$20 mg) using the rapid quenching technique described in Ref. 5. The binary Te-Au specimens were quenched directly from a carbon crucible, while the specimens containing Fe and Mn were melted on an alumina insert placed inside the carbon crucible in order to prevent the formation of carbides. All specimens were quenched from the liquid state onto a flat copper substrate at room temperature. The samples obtained by this technique are irregularly shaped foils about 25 mm long and 8 mm wide, whose thickness is not uniform, but is in general less than 10μ. Since, according to Ref. 6, the quenching rate is not exactly reproducable, each foil to be used for magnetoresistance, resistivity, or thermoelectric power measurements, was scanned on a Norelco diffractometer

TABLE I

Materials used in alloy preparation

Material	Supplier	Purity
Tellurium	American Smelting and Refining Company	99.999 + %
Gold	Jarrell Ash Co Handy and Harmon	99.99 %
Iron	Plastic Metals	Electrolytic (99.9%)
Manganese		Electrolytic

using CuKα radiation through a range of 2θ angles from 20° to 40°. Within this interval only the (100) peak of the simple cubic pattern should appear, and foils containing extraneous peaks were discarded. For lattice parameter and superconductivity work, the material was carefully scraped from the copper strip yielding an extremely fine powder. For resistivity, thermoelectric power, and magnetoresistance measurements, the foils were transferred to a resin called "quickmount" by the following procedure. The copper strip containing the specimen was placed securely in a teflon mold, and the epoxy resin, mixed in a volume ratio of 2:1 (powder to liquid) was poured into the mold on top of the specimen. When the resin hardened, the entire assembly was removed from the mold, and the copper strip was peeled off, leaving the specimen firmly attached to the epoxy.

C. Lattice Spacings

The lattice spacings of all alloys studied were determined using CuKα radiation and a 114.6 mm Debye-Scherrer powder camera. The powder scraped from the copper substrate following quenching was placed in a 0.3 mm glass capillary tube and exposed to x-rays for 4 to 6 hours. Care was taken during removal of the sample material from the substrate to insure that none of the substrate material was carried with the powder. In general, between 9 and 12 diffraction lines were visible on the film, and the lattice spacings were determined by extrapolation against the Nelson-Reily function. The weighted average wavelength for $K\alpha_1$ and $K\alpha_2$ was used since none of the high angle

diffraction lines were resolved.

D. Superconducting Transition Temperature

The superconducting transition temperature was measured using the probe shown in Fig. 1 and the apparatus shown in Fig. 2. The sample rests inside the specimen coil (~1200 turns of copper wire) and when it transforms to the superconducting state, the exclusion of the flux from the specimen (Meissner effect) causes a change in the inductance of the specimen coil. This causes an electrical imbalance of a Wheatstone bridge circuit resulting in the appearance of a signal at the input to a lock-in amplifier. At this point, two modes of operation are possible. The amplifier can be caused to emit a D.C. signal which is proportional either to the amplitude of the input signal, or to the phase difference between the input signal and a reference signal. It has been found that the latter method of operation, called the phase mode, is the most sensitive and makes best use of the features of the lock-in amplifier. The advantages of the inductance method of measurement are a consequence of the lack of any physical connections to the sample, and the tolerance of any physical shape of condition of the sample. It has been found that by using about 5 mg of material (4 to 8 foils) a sufficiently large signal at the superconducting transition temperature is observed. It can be seen from the diagram of the probe (Fig. 1) that both coils shown in Fig. 2 are maintained at low temperature though only one contains a sample. These two coils are nearly identical and it has been found that maintaining them at the same temperature almost entirely eliminates drift

due to either dimentional changes in the coils or temperature variation of the resistance.

The temperature was measured by means of a Honeywell Germanium thermometer shown in Fig. 1. A current of 0.01 ma was passed through the thermometer, and the output voltage was connected to the x-axis of a Mosley x-y recorder. The thermometer was calibrated below 4.2°K against the He vapor pressure in the closed probe shown in Fig. 1, using "1958 He^4 vapor pressure scale of temperatures."[7]

The probe (modeled after a design described in Ref. 8) is easy to use and consumes a relatively small quantity of liquid He. The sample chamber of the probe, containing three specimens, the Germanium thermometer, and the He vapor pressure chamber, is separated from the He bath by a vacuum jacket, allowing heat flow only through the thermal leak just below the heater. In using this probe it is only necessary to pump the liquid He bath down to 1.5°K once. The temperature is then cycled using the internal heater, and holding the bath at 1.5°K. This makes it possible to cycle the sample temperature rapidly since there is very little thermal inertia. It has been found in practice that the designed heat leak is somewhat inadequate, and is usually supplemented by a partial pressure of about 1 mm of He in the vacuum jacket.

E. Thermoelectric Power

Thermoelectric power measurements were performed on specimens mounted on epoxy and placed in the holder shown in Fig. 3, positioning the

thermocouple beads over the thickest portions of the specimen. The thermoelectric power of the specimen against copper was measured using a Leeds and Northrup type K-5 potentiometer and a sample temperature gradiant of 4-7°K. It was found that the scatter in the measurements was minimized if the mean temperature was allowed to rise extremely slowly; consequently, a measurement from liquid nitrogen temperature to room temperature required about 48 hours. The absolute accuracy of this method of measurement is estimated to be ±2%.

F. Magnetoresistance

The samples for measuring the transverse magnetoresistance were identical to those used for thermoelectric power measurements. The samples were placed in the probe shown in Fig. 4 which was then centered in a Varian 12" magnet. All measurements were made with the specimen submerged in a liquid He bath at atmospheric pressure. Due to thermal fluctuations at the top of the probe, it was necessary to make a zero field measurement before and after each measurement with the magnetic field applied. In each case the actual resistance at zero field was taken to be the average of these two readings. Each specimen was measured up to a field of 8 KG using a Leeds and Northrup guarded potentiometer for the resistance and a Varian proton resonance device for the magnetic field.

G. Electrical Resistance

The resistance as a function of temperature was measured using a probe very similar to the one shown in Fig. 4. A current of from 1 to 20 ma from a Princeton Applied Research Model TC-100 constant current source was passed through the specimen, and the potential output was connected to the y-axis of a Mosley x-y recorder. A copper constantan thermocouple in physical contact with the specimen was used to drive the x-axis of the recorder. The probe was then cooled rapidly to liquid nitrogen temperature and allowed to warm up at the rate of $\sim 1^{\circ}K$ per minute while the measurement was being performed. To correct for the non-linearity of the thermocouple, the data were replotted after converting emf to temperature.

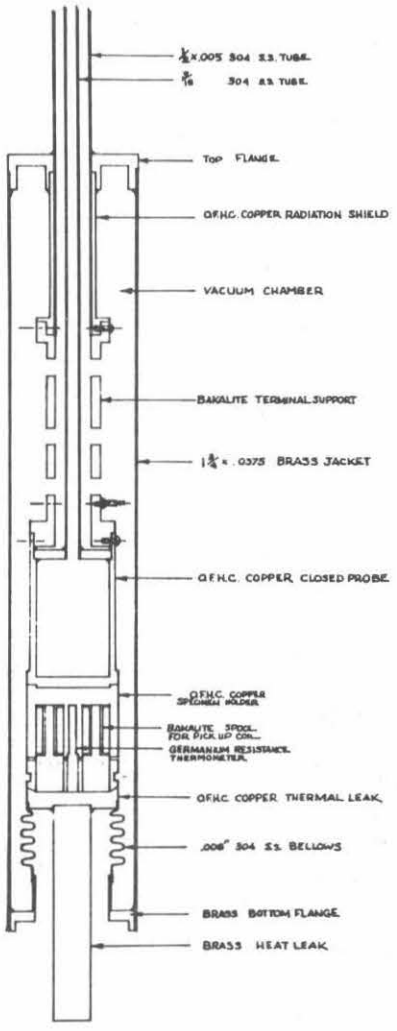

Fig. 1 Section of low temperature probe used to measure superconducting transition temperatures

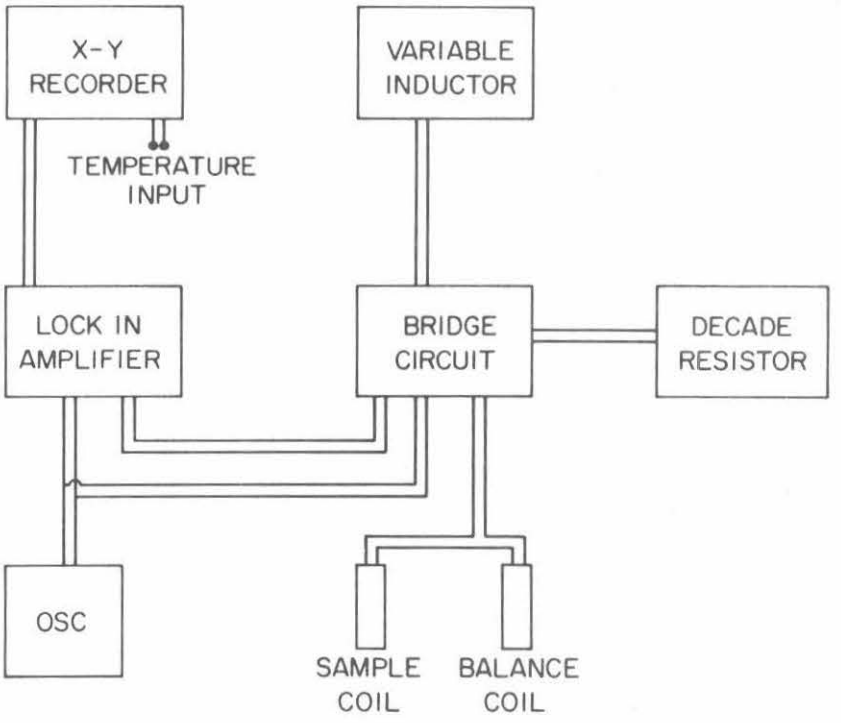

Fig. 2 Electrical arrangement of equipment for measuring superconducting transition temperatures

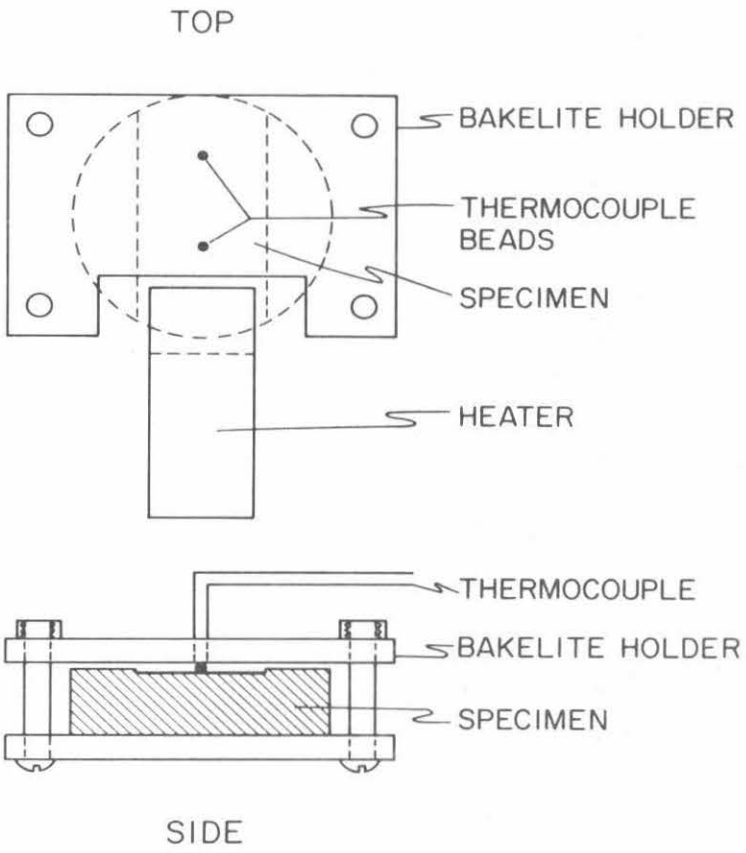

Fig. 3 Specimen holder for measurement of thermoelectric power

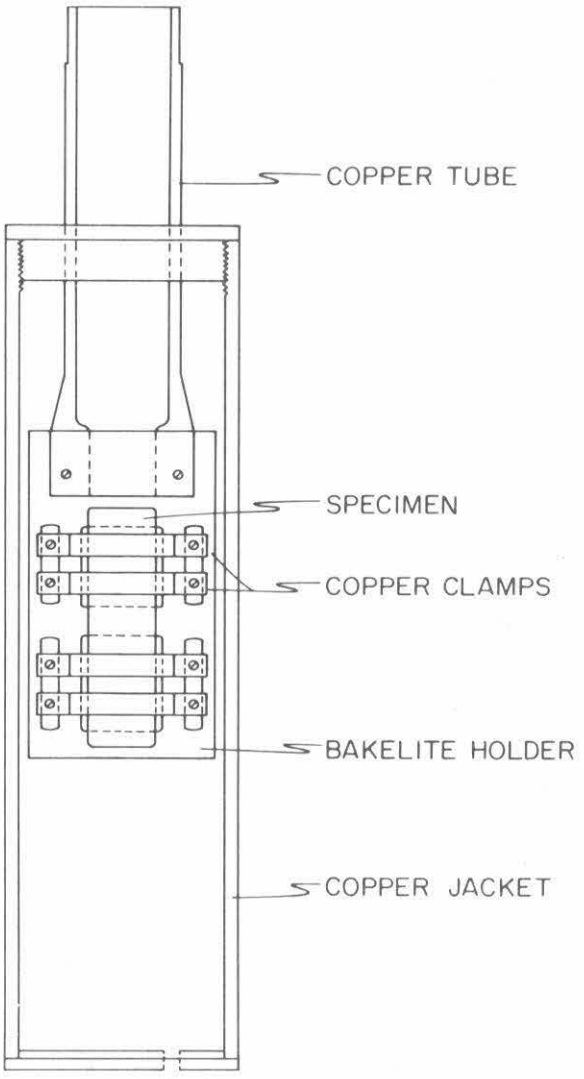

Fig. 4 Section of low temperature probe for measurement of magneto-resistance

III. EXPERIMENTAL RESULTS

A. Thermoelectric Power

The thermoelectric power was measured as a function of Te concentration and as a function of temperature. As a function of temperature the thermoelectric power of all compositions studied was found to be substantially linear between 140 and 300°K. A typical example for the alloy $Te_{77.3}Au_{22.7}$ is shown in Fig. 5. The thermoelectric power as a function of temperature for a given composition can be described by the following empirical formula,

$$S = A + BT \qquad (1)$$

where S is the absolute thermoelectric power, T is the absolute temperature and A and B are constants. The variations of A and B as a function of concentration are shown in Figs. 6 and 7 respectively. The anomalies which occur at approximately 70 at % Te and 80 at % Te should be noted, since these recur in measurements of other properties to be discussed below. Figure 8 shows the absolute thermoelectric power as a function of concentration at 290°K. Again the anomalous behavior occurring at 70 and 80 at % Te should be noted. The experimental error involved in the measurements presented may be divided into two sources. The first and most important source of scatter is due to the lack of reproducibility of the quenching rate. The results indicate that this affects the parameter A more than B. The second source of scatter is due to the error involved in the measurements and is estimated to be less than 2%.

It seems this uncertainity is small enough to be ignored compared with the first source mentioned. Figure 9 shows the thermoelectric power of three foils of $Te_{66.7}Au_{33.3}$ each mounted on a different type of epoxy resin. The slopes and intercepts of the three samples seem to fall within the scatter due to the uncertainity in quenching rate, indicating that the nature of the mounting has no substantial effect on the measurement.

B. Superconducting Transition Temperature

Figure 10 shows a typical plot of resistance versus temperature for the alloy $Te_{66.7}Au_{33.3}$ as it passes through the superconducting transition. The resistance drops almost exactly to zero below the critical temperature, indicating that the transitions observed in this study by the induction method are indeed superconducting transitions. Figure 11 shows the results of measurements of the superconducting transition temperature vs Te concentration for the binary Te-Au system[9]. In all cases the transitions were about 1°K in width, and the temperatures shown are for the onset of superconductivity. The uncertainity in the temperature measurement is estimated to be 0.1°K, taking into account scatter due to quenching rate, and error in temperature measurement. The maximum and minimum occurring at 70at% and 80at% Te respectively coincide with the anomalies in the thermoelectric power measurements. Figures 12, 13, and 14 present the results of measurements of the superconducting transition temperatures of $(Te_{65}Au_{35})_{100-x}Fe_x$, $(Te_{70}Au_{30})_{100-x}Fe_x$, and $(Te_{75}Au_{25})_{100-x}Fe_x$. The results presented for $(Te_{70}Au_{30})_{100-x}Fe_x$ contain each experimental point

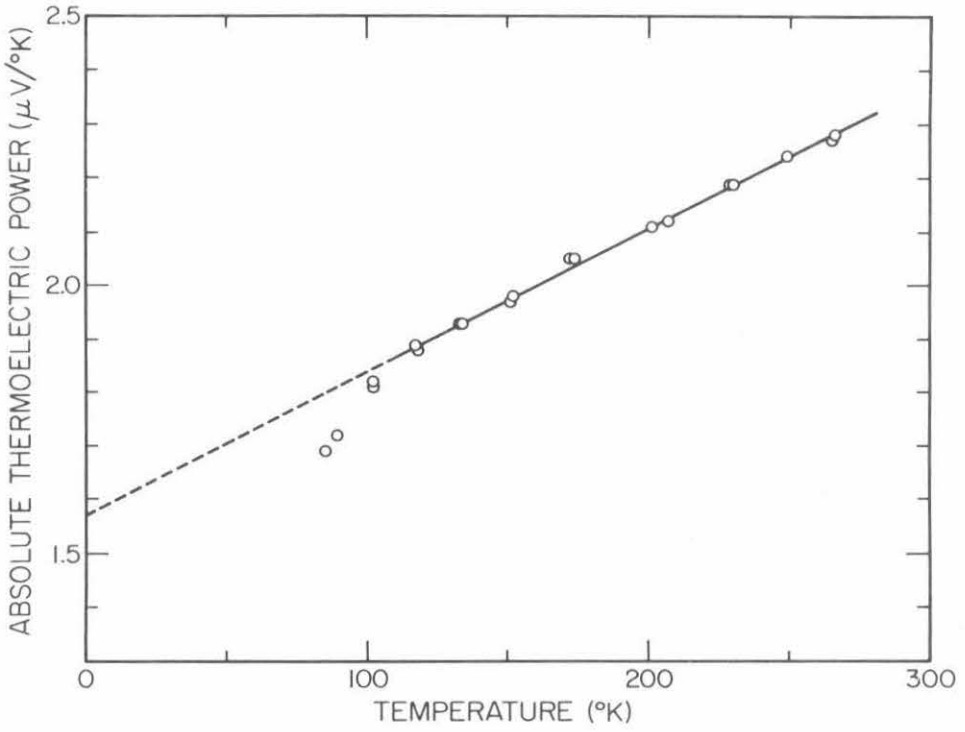

Fig. 5 Absolute thermoelectric power of the simple cubic alloy $Te_{77.3}Au_{22.7}$ as a function of temperature

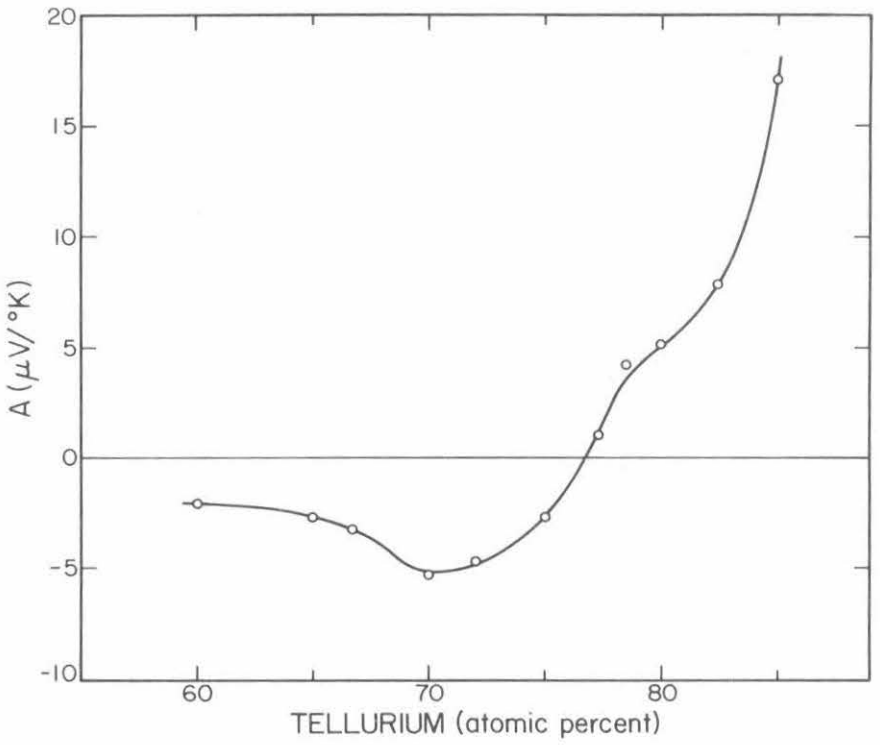

Fig. 6 Composition dependence of parameter A in Eq. (1)

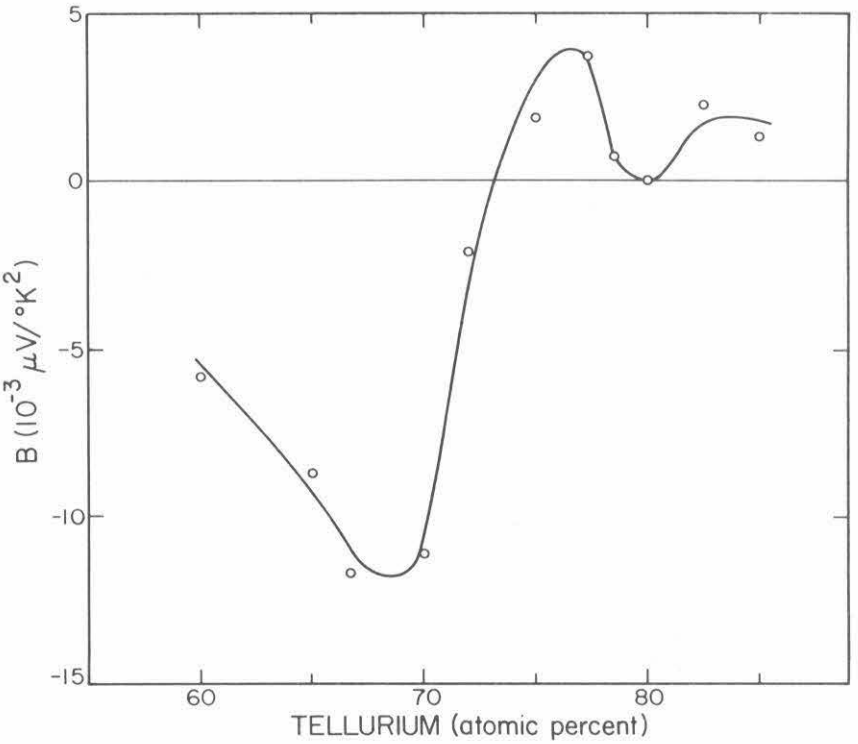

Fig. 7 Composition dependence of parameter B in Eq. (1)

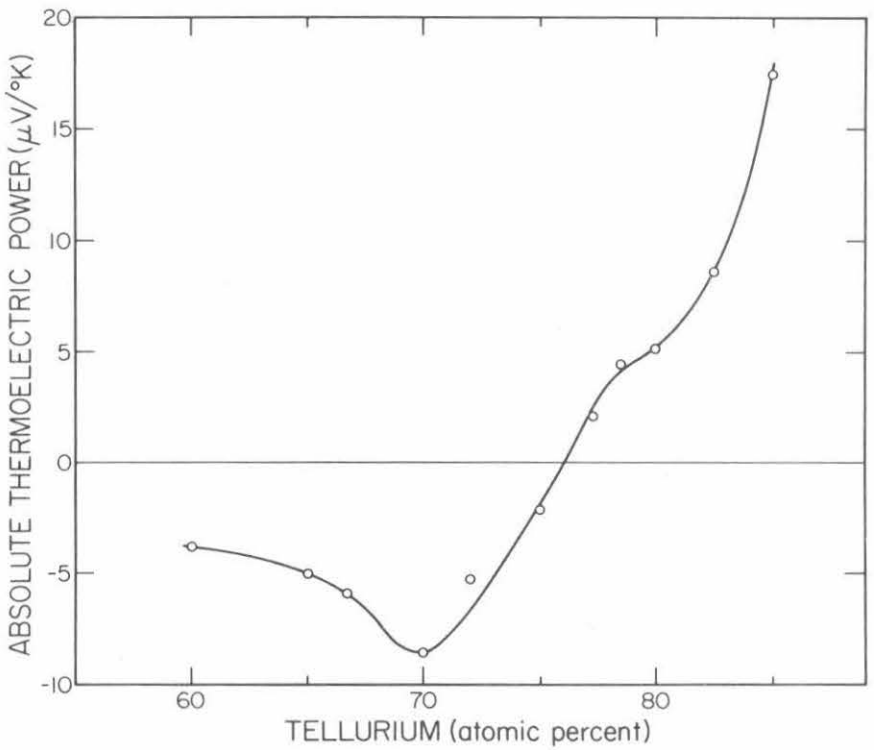

Fig. 8 Absolute thermoelectric power of simple cubic Te-Au alloys at 290°K

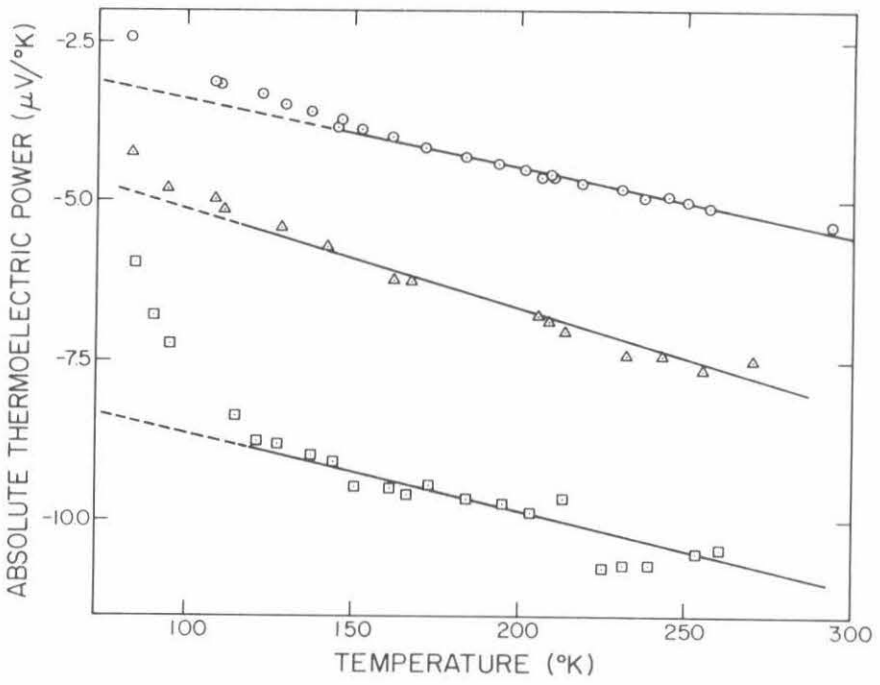

Fig. 9 Absolute thermoelectric power of the simple cubic alloy $Te_{66.7}Au_{33.3}$ mounted on Bonding Agent R-313 (⊙), mounted on quickmount (△), mounted on low-temperature epoxy composed of Bakalete #2774 and Versamia #140 (⊡)

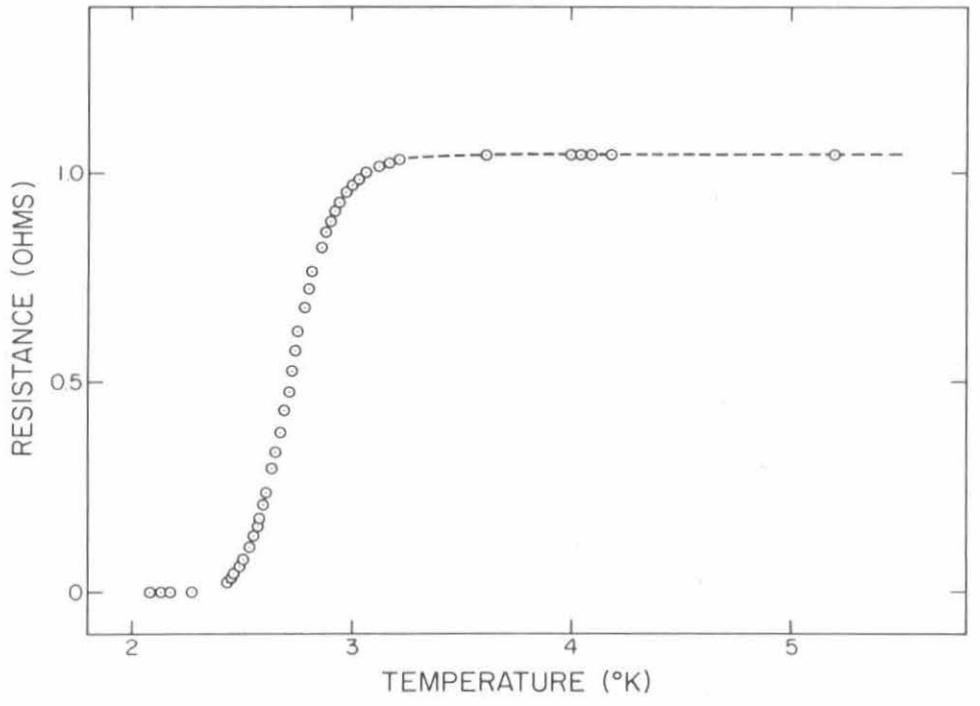

Fig. 10 Electrical resistance of the simple cubic alloy $Te_{66.7}Au_{33.3}$ near the superconducting transition

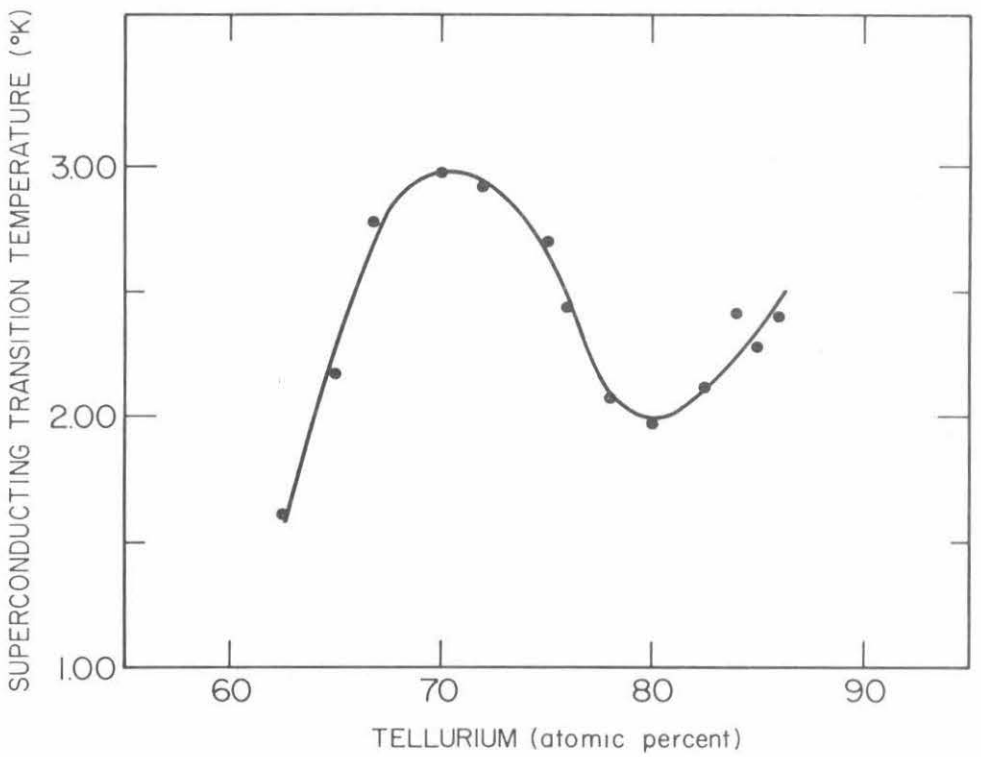

Fig. 11 Superconducting transition temperature of simple cubic Te-Au alloys

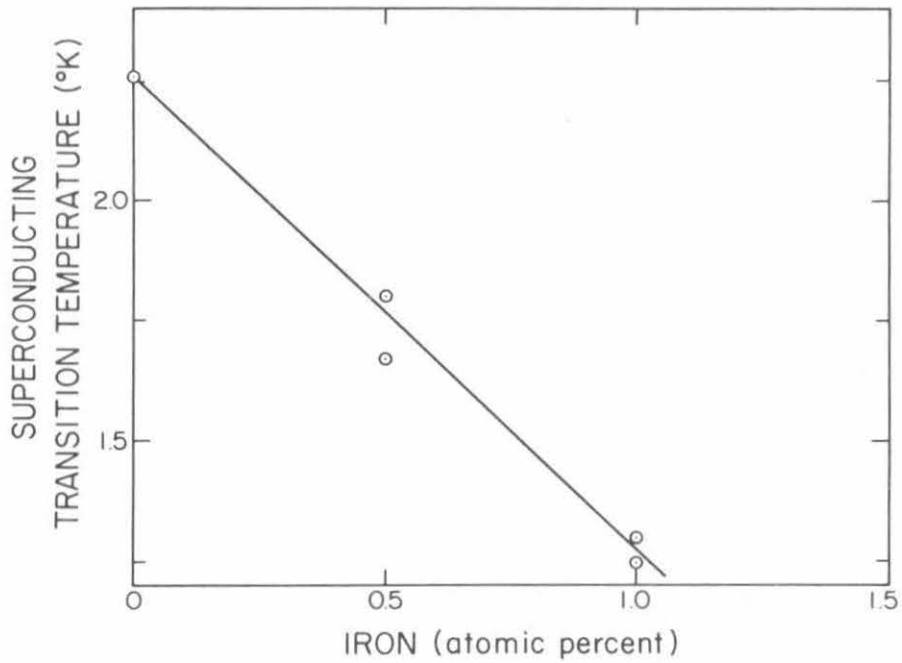

Fig. 12 Superconducting transition temperature of the simple cubic alloys $(Te_{65}Au_{35})_{100-x}Fe_x$

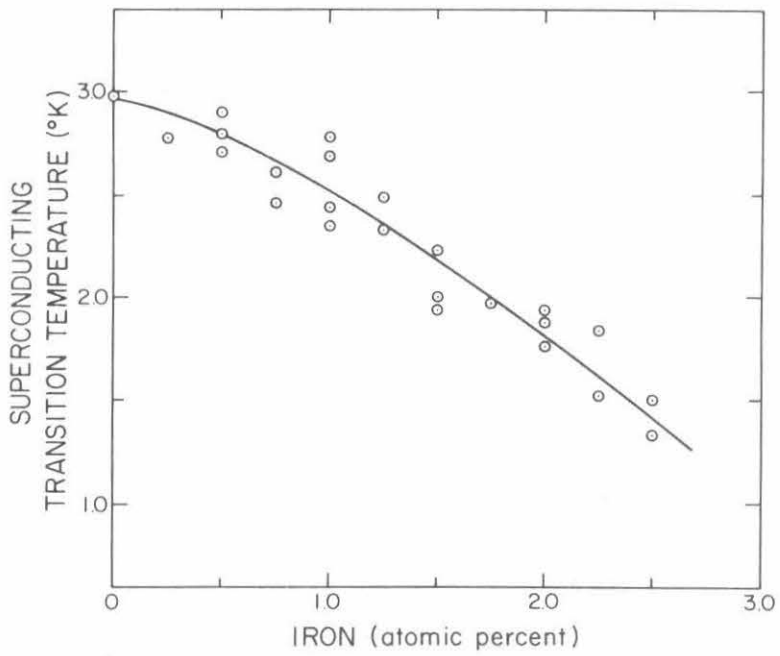

Fig. 13 Superconducting transition temperature of the simple cubic alloys $(Te_{70}Au_{30})_{100-x}Fe_x$

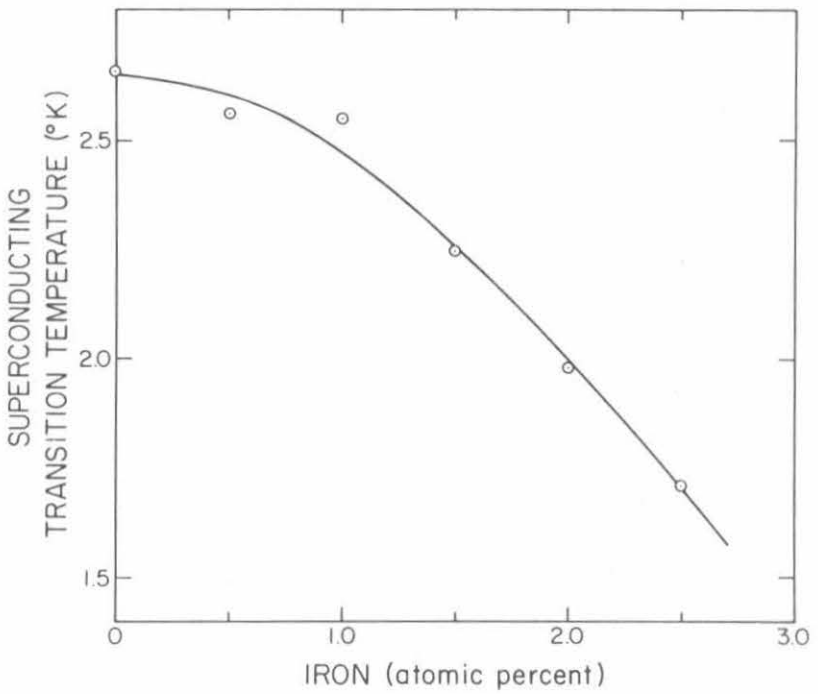

Fig. 14 Superconducting transition temperature of the simple cubic alloys $(Te_{75}Au_{25})_{100-x}Fe_x$

measured, in order to indicate the scatter and the uncertainity involved in the measurements. The results presented for the systems Te-Au, $(Te_{65}Au_{35})_{100-x}Fe_x$, and $(Te_{75}Au_{25})_{100-x}Fe_x$ are the average of from 3 to 6 measurements at each composition. The most important feature of these results is the relatively small effect of Fe on the transition temperature.

The results of measurements on the alloys $(Te_{70}Au_{30})_{100-x}Mn_x$ are not presented graphically since it was found that the superconducting transition temperature was surpressed below 1.3°K by the addition of only 0.5 at% Mn. This implies that the slope of transition temperature vs Mn concentration is at least 2.5°K per at% Mn. This should be compared to the slope of the transition temperature vs Fe concentration for $(Te_{70}Au_{30})_{100-x}Fe_x$ which is roughly 0.6°K/at% Fe.

C. Lattice Parameter

Figure 15 shows a diffractometer trace of the alloy $Te_{66.7}Au_{33.3}$ over a range of 2θ angles from 20° to 120°. It can be concluded from this pattern, that the Te-Au alloys have a simple cubic crystal structure and are essentially single phase. The results of measurements of the lattice parameters for the binary Te-Au system are presented in Fig. 16. These results seem to fall in two linear portions with a break at around 68 at% Te. Above 68 at% Te, the lattice spacing increases with increasing Te content at a rate of 7.3×10^{-3} Å per at% Te, and below 68 at% Te the increase slows to 2.3×10^{-3} Å per at% Te. The results of measurement of lattice spacings for the systems $(Te_{80}Au_{20})_{100-x}Fe_x$, and

$(Te_{75}Au_{25})_{100-x}Fe_x$ are shown in Fig. 17. The lattice parameter for the second system mentioned also seems to fall in two linear portions with a break at approximately 3 at% Fe. Above this concentration the lattice spacings decrease with increasing Fe content at a rate of 6.3×10^{-3} Å per at% Fe. Below this concentration the decrease is 13.5×10^{-3} Å per at% Fe. The results of lattice spacings measurements on the systems $(Te_{70}Au_{30})_{100-x}Fe_x$, $(Te_{65}Au_{35})_{100-x}Fe_x$ and $(Te_{60}Au_{40})_{100-x}Fe_x$ are presented in Fig. 18. In all three cases the lattice parameter decreases linearly with increasing Fe content with slopes of 5.8×10^{-3} Å per at% Fe, 3.8×10^{-3} Å per at% Fe and 2.6×10^{-3} Å per at% Fe respectively. The results of lattice parameter measurements on the alloys $(Te_{70}Au_{30})_{100-x}Mn_x$ are shown in Fig. 19. For the limited region studied, the lattice parameter decreases linearly with increasing Mn concentration with a slope of 10.3×10^{-3} Å per at% Mn. The results of all the lattice parameter measurements are summarized in Table II.

D. Magnetoresistance

The results of magnetoresistance measurements performed on specimens of $(Te_{70}Au_{30})_{98.5}Fe_{1.5}$ and $(Te_{70}Au_{30})_{98.5}Mn_{1.5}$ are shown in Fig. 20. At 8 KG, the sample containing Fe as an impurity has a magnetoresistance of $+23 \times 10^{-5}$, while the specimen containing Mn as the impurity shows -11×10^{-5}. The significance of this measurement lies in the negative contribution to the magnetoresistance when Fe is replaced by Mn. The accuracy of the measurements shown is estimated to be $\pm 5 \times 10^{-5}$.

TABLE II

Summary of Lattice Parameter Data

System	Slope of Lattice Parameter (10^{-3} Å/at% x)	Extrapolated size of Metal x
$(Au_{30}Te_{70})_{100-x}Mn_x$	- 10.3	1.97 Å
$(Au_{20}Te_{80})_{100-x}Fe_x$	- 12.5	1.80 Å
$(Au_{25}Te_{75})_{100-x}Fe_x$	- 13.5	1.68 Å (x<3)
$(Au_{25}Te_{75})_{100-x}Fe_x$	- 6.3	2.38 Å (x>3)
$(Au_{30}Te_{70})_{100-x}Fe_x$	- 5.8	2.40 Å
$(Au_{35}Te_{65})_{100-x}Fe_x$	- 3.8	2.58 Å
$(Au_{40}Te_{60})_{100-x}Fe_x$	- 2.6	2.68 Å
$Au_{100-x}Te_x$	+ 2.3	3.07 Å (x<68)
$Au_{100-x}Te_x$	+ 7.3	3.21 Å (x>68)

E. Electrical Resistance

Figure 21 is a typical plot of the resistance of a foil of $Te_{66.7}Au_{33.3}$ as a function of temperature. The resistance increases almost linearly with temperature except in the region around room temperature where the increase becomes much faster than linear. Several specimens of this composition were studied and the resistance vs temperature curves have essentially the same shape, except for some variations in the slopes of the linear portions.

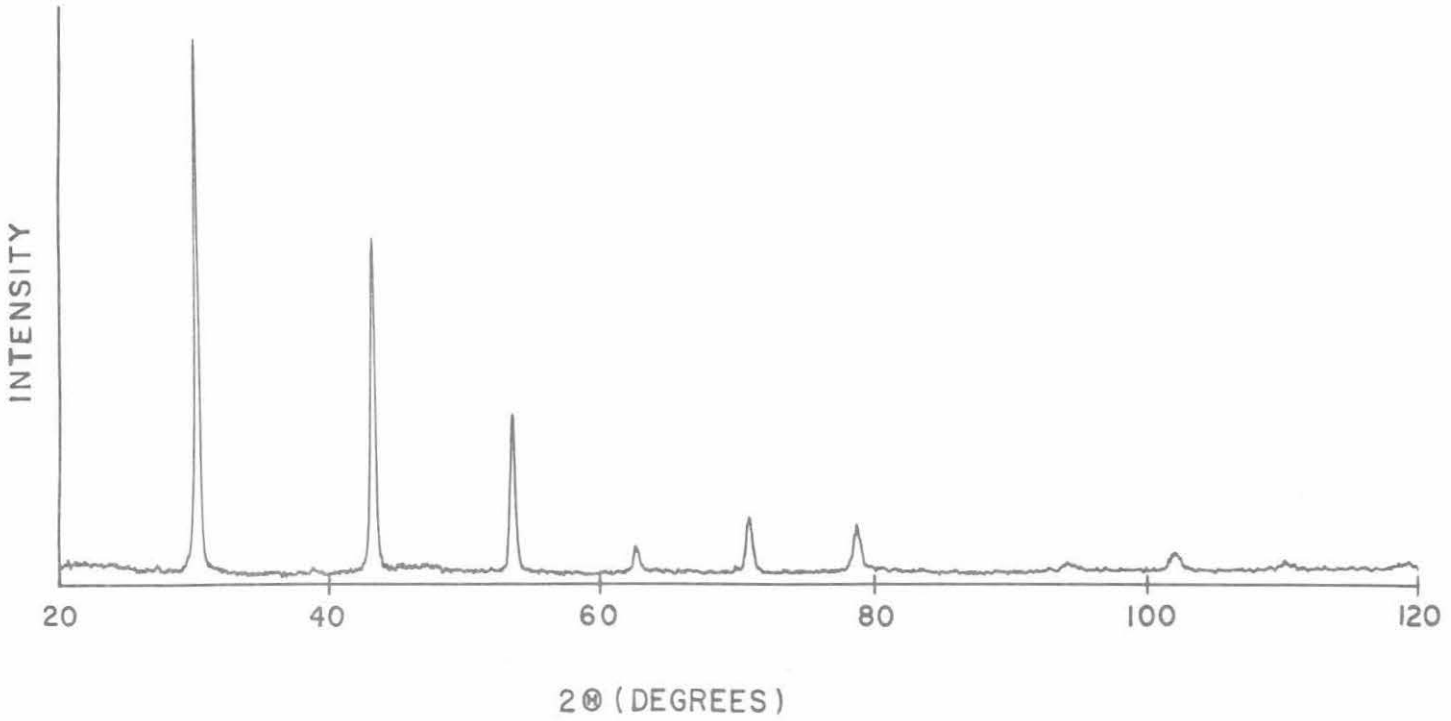

Fig. 15. X-ray diffraction pattern of the simple cubic alloy $Te_{66.7}Au_{33.3}$

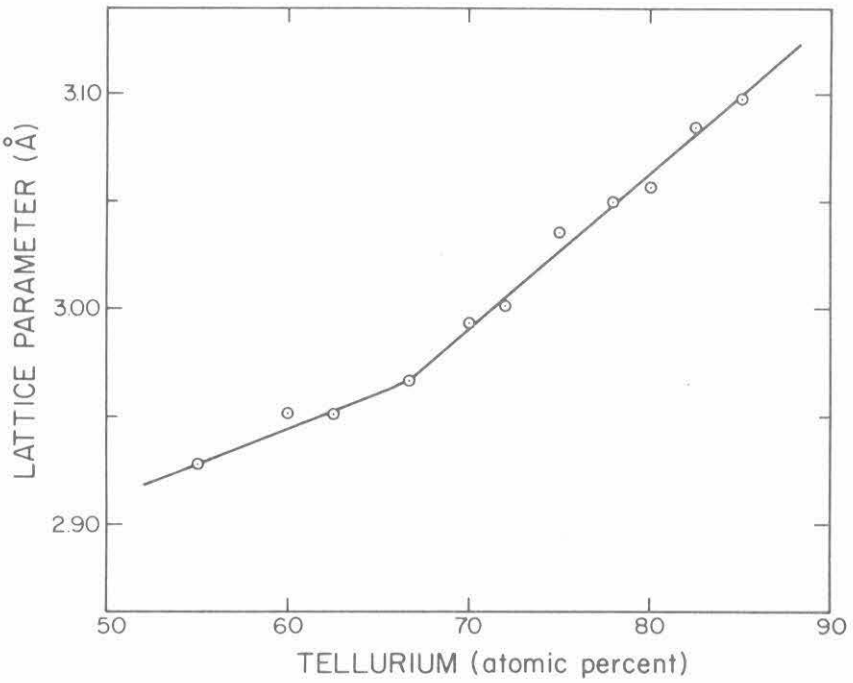

Fig. 16 Lattice parameter of the simple cubic Te-Au alloys

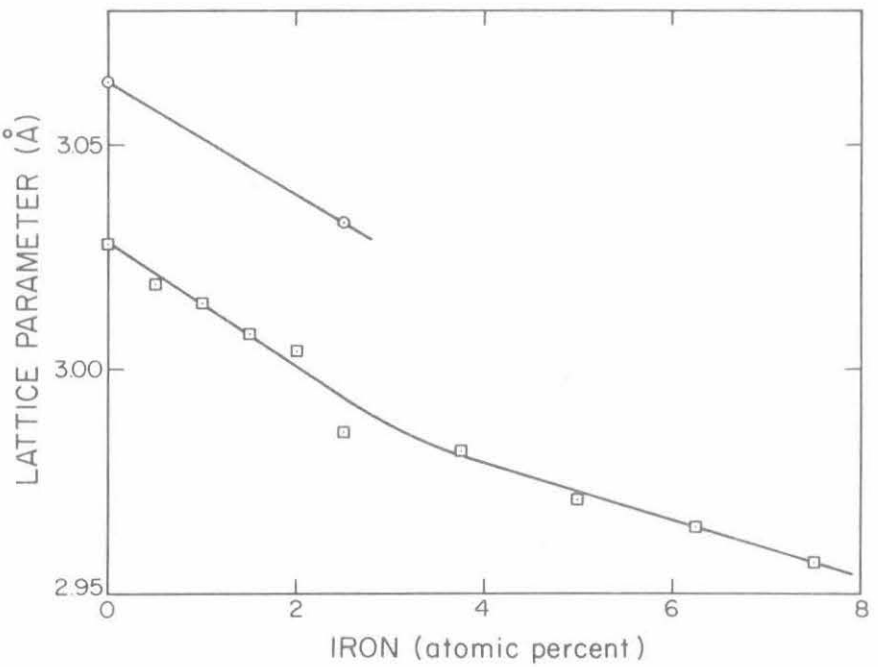

Fig. 17 Lattice parameter of the simple cubic alloys $(Te_{80}Au_{20})_{100-x}Fe_x$ (⊙), and $(Te_{75}Au_{25})_{100-x}Fe_x$ (⊡)

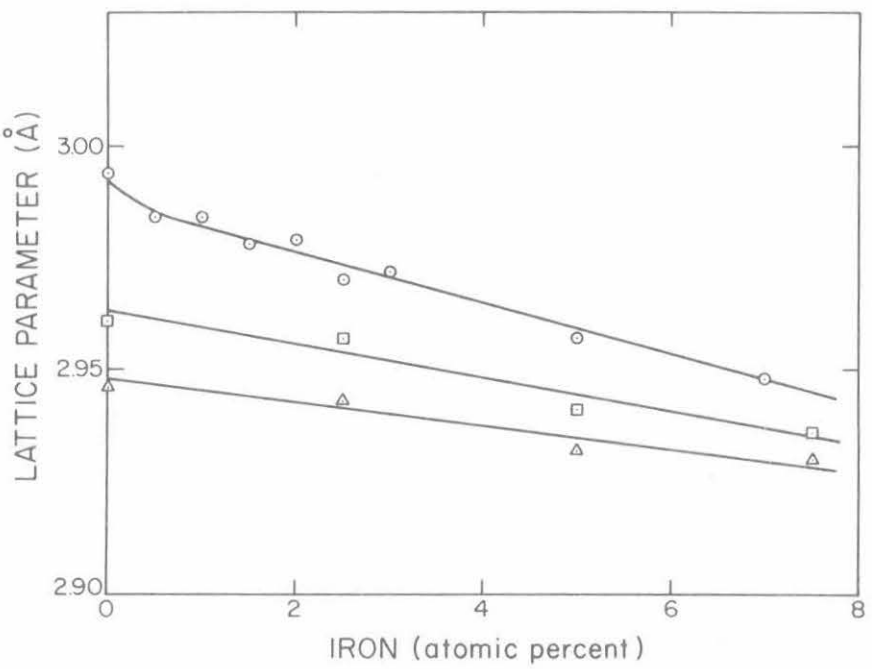

Fig. 18 Lattice parameter of the simple cubic alloys $(Te_{70}Au_{30})_{100-x}Fe_x$ (⊙), $(Te_{65}Au_{35})_{100-x}Fe_x$ (⊡), and $(Te_{60}Au_{40})_{100-x}Fe_x$ (△)

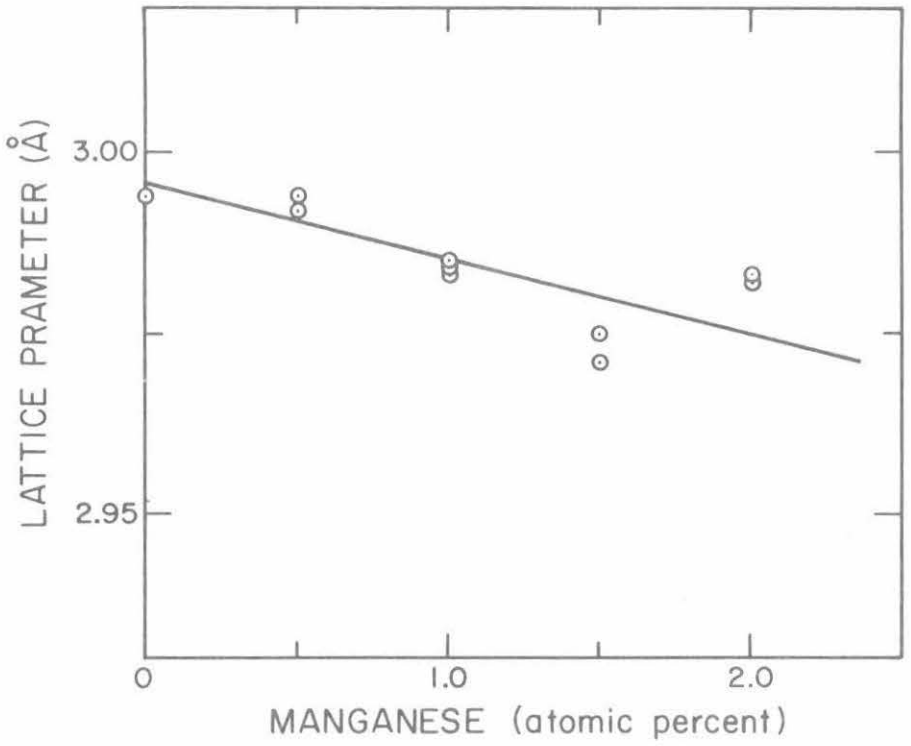

Fig. 19 Lattice parameter of the simple cubic alloys $(Te_{70}Au_{30})_{100-x}Mn_x$

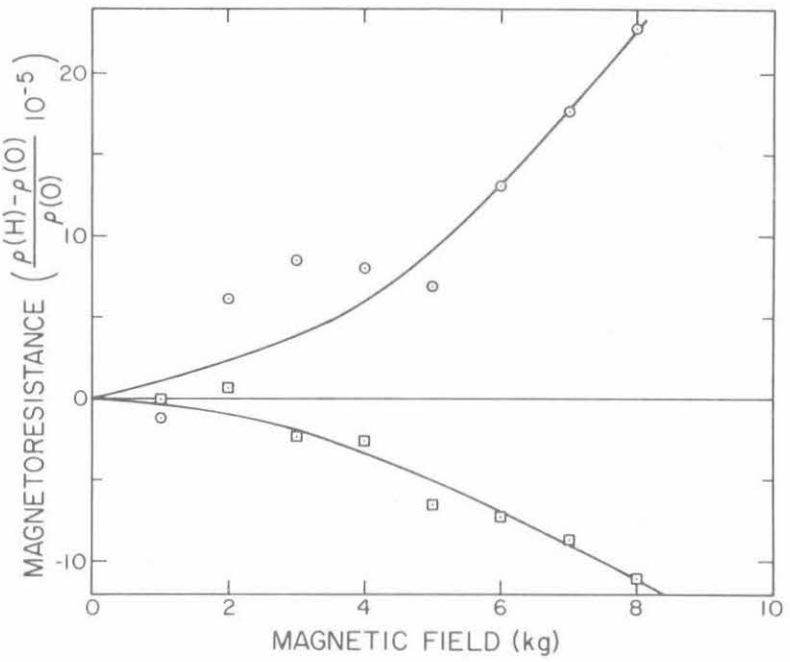

Fig. 20 Transverse magnetoresistance of the simple cubic alloys $(Te_{70}Au_{30})_{98.5}Fe_{1.5}$ (⊙), and $(Te_{70}Au_{30})_{98.5}Mn_{1.5}$ (⊡)

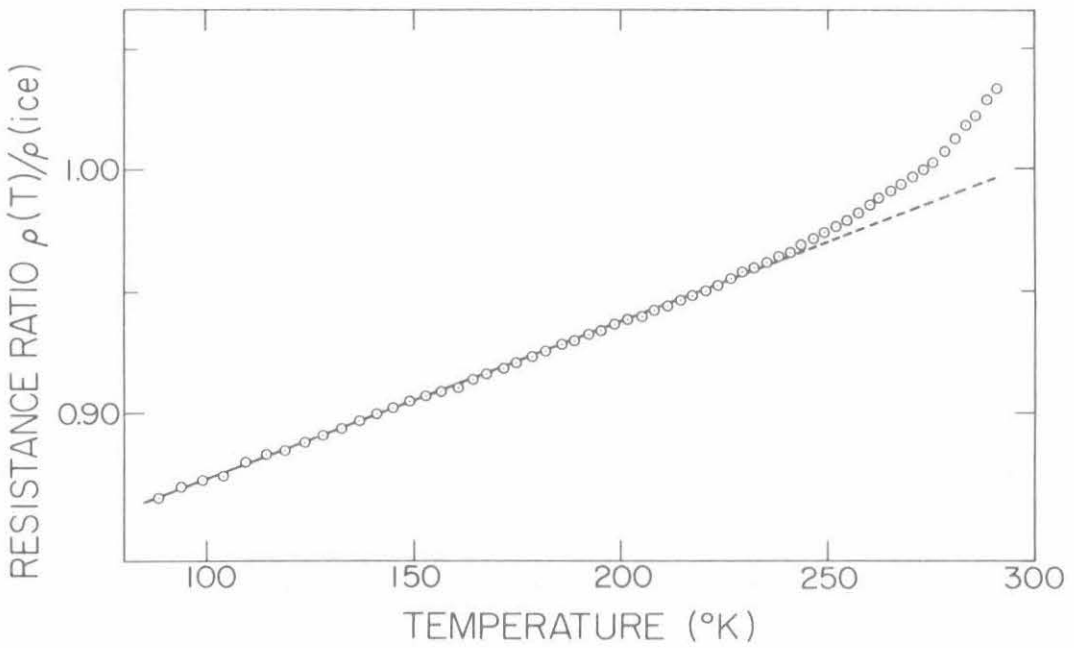

Fig. 21 Electrical resistance of the simple cubic alloy $Te_{66.7}Au_{33.3}$ as a function of temperature

IV DISCUSSION

A. Relationship Between Equilibrium $AuTe_2$ and the Simple Cubic Crystal Structure

As shown in the equilibrium phase diagram[10] reproduced in Fig. 22, the only compound in the Te-Au system is $AuTe_2$, which exhibits no range of homogenity. Equilibrium $AuTe_2$ has the monoclinic crystal structure of the mineral calaverite[11], with $a_o = 7.18$ Å, $b_o = 4.40$ Å, $c_o = 5.07$ Å and $\beta = 90^\circ\ 30'$. Gold atoms are located at 0,0,0, and 1/2, 1/2, 0, and Te atoms occupy positions (m,0,p), ($\bar{m}$,0,$\bar{p}$), (m+1/2, 1/2, p) (1/2-m, 1/2,$\bar{p}$), where m = 0.69 and p = 0.29. In clearer notation this places Te atoms at (0.69, 0, 0.29), (0.31, 0, 0.71), (0.19, 1/2, 0.29), and (0.81, 1/2, 0.71). The type, number, and distance of the neighbors are shown in Table III. As pointed out by Luo and Klement[2], if the Au and Te atoms are distributed at random, this structure can be viewed as a slightly distorted simple cubic lattice. For an Au atom, the three planes formed by the six nearest neighbors intersect at the Au site with angles of $83^\circ\ 56'$, $96^\circ\ 59'$, and $96^\circ\ 59'$. The three planes formed by the neighbors of a Te atom intersect 0.42 Å from the Te site with angles of $87^\circ\ 10'$, $86^\circ\ 50'$, and $86^\circ\ 50'$. The interatomic distance obtained by averaging all 12 spacings listed in Table III is 2.98 Å, which is very close to the lattice spacing of 2.97 Å experimentally determined for simple cubic $AuTe_2$.

TABLE III

Nearest neighbor arrangement in equilibrium $AuTe_2$

Site	Number of Neighbors	Type	Distance
Au	2	Te	2.68Å
	2	Te	2.98Å
	2	Te	2.98Å
Te	2	Te	3.19Å
	1	Te	3.46Å
	2	Au	2.98Å
	1	Au	2.68Å

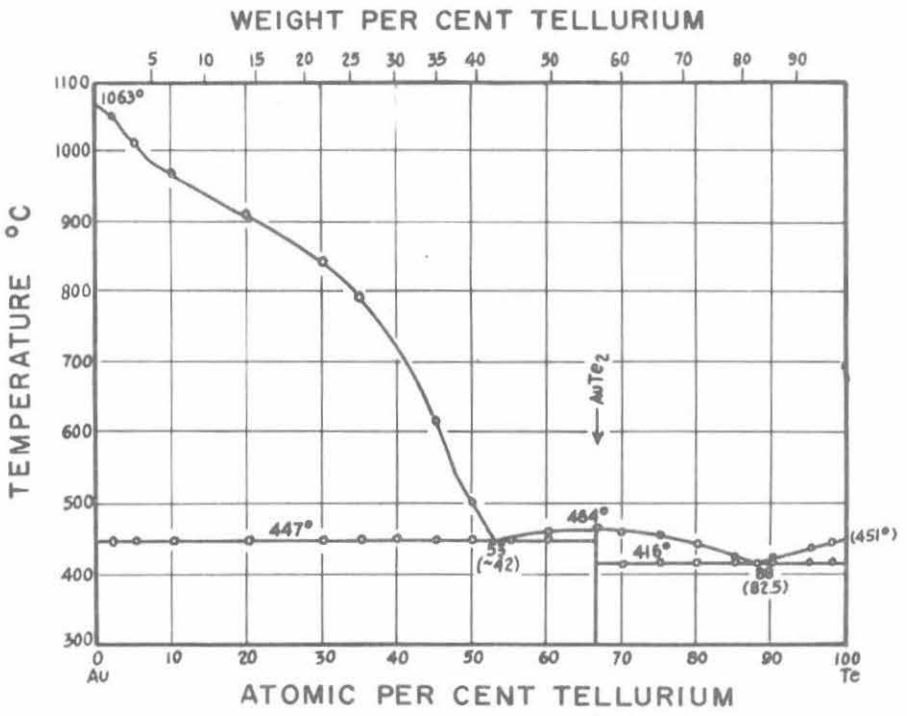

Fig. 22 Equilibrium phase, diagram for the binary Te-Au system (Ref. 10)

B. Brillouin Zones for the Simple Cubic Structure

The Brillouin zones for any crystal structure with one atom per unit cell may be constructed directly from the reciprocal lattice[12,13]. The Brillouin zone boundaries are defined by the $\bar{k}$ vectors in momentum space which satisfy the following relationship,

$$2\bar{k} \cdot \bar{G} + |G|^2 = 0 \qquad (2)$$

where $\bar{k}$ is the wave vector of an electron and $\bar{G}$ is a reciprocal lattice vector. This equation describes a geometrical construction in reciprocal space consisting of the plane which perpendicularly bisects each reciprocal lattice vector. It can be shown[12] that this equation also describes the condition for a Bragg reflection to occur in a crystal lattice.

The geometrical structure of the Brillouin zones for the simple cubic structure is relatively simple compared to that for hexagonal and other cubic structure types. The first Brillouin zone is simply a cube of edge $\frac{2\pi}{a}$ in momentum space, while the second zone is bounded by a dodecahedron whose six pairs of parallel sides are spaced $\frac{2\sqrt{2}\pi}{a}$ apart. The higher zones become too complicated for verbal description, but are shown in detail in Fig. 23, taken from Brillouin's book[14].

C. Proposed Band Structure Model

The model to be described in this section, which is based primarily on the nearly free electron theory (NFET), will be used to interpret the experimental

measurements in terms of an interaction between the Fermi surface and the Brillouin zone boundaries.

If one makes the assumption that the conduction electrons in a solid see only a weak periodic potential, then it is possible to obtain approximate solutions to Schroedinger's equation[15-18]. Probably, the most significant result of this assumption is that the energy expressed as a function of wave vector, E(k), is unchanged from the free electron result except where the wave vector $\bar{k}$ lies near a Brillouin zone boundary. In the region of a Brillouin zone boundary, the contours of constant energy are bent toward the boundary as though attracted by it. Because the Bragg condition is satisfied whenever a contour of constant energy meets a boundary, the contour at the boundary must satisfy the following condition,

$$\bar{\nabla}_k E(\bar{k}) \cdot \bar{G} = 0 \qquad (3)$$

where $\bar{G}$ is the reciprocal lattice vector giving rise to the boundary under consideration. Since the Bragg condition is satisfied, it follows that the wave function in a direction parallel to G must be composed of standing waves. This implies that there can be no energy transmission in the direction of $\bar{G}$, requiring that the group velocity satisfy

$$\bar{V}_g \cdot \bar{G} = 0 \qquad (4)$$

We know that

$$\bar{V}_g = \bar{\nabla}_k \omega(\bar{k}) \qquad (5)$$

and for free electrons

$$\omega(\bar{k}) = \frac{E(\bar{k})}{\hbar} \tag{6}$$

When equations (5) and (6) are substituted into equation (4) we find

$$\frac{1}{\hbar} \bar{\nabla}_k E(\bar{k}) \cdot \bar{G} = 0 \tag{7}$$

which is the origin of equation (3).

The nearly free electron model seems to provide a satisfactory explanation for the transport properties in many metals and alloys. This is rather surprising, since it appears that the potential encountered by an itinerate electron is hardly a weak one. It seems, in fact, that the potential near the core would be extremely deep, and the assumption made at the beginning of this chapter might be entirely invalid. The best explanation available to account for the success of this theory has been provided by Harrison[19]. His pseudo potential theory indicates that the potential due to electrons in lower eigenstates (core electrons) effectively cancels most of the potential due to the nucleous, with the result that the conduction electrons do indeed see a weak periodic potential.

Using the results of the nearly free electron theory, the following description of the topology of the Fermi surface will be used to interpret the experimental data. From NFET we know that contours of constant energy in $\bar{k}$ space are described by (except near a zone boundary)

$$E(\bar{k}) = \frac{\hbar^2}{2m} (k^2_x + k^2_y + k^2_z) = C \qquad (8)$$

where k_x, k_y, and k_z are the components of the electron wavevector, and C is a constant. The surfaces in $\bar{k}$ space described by Eq. (8) are spheres centered about $\bar{k} = 0$. This implies that the Fermi surface is essentially spherical except in the immediate vicinity of a zone boundary where it distorts in a manner consistent with the conditions described in Eq. (3). The qualitative hypothesis to be used in the remainder of the discussion is the following. At the lower limit of Te concentration the Fermi surface is essentially a sphere located largely in the second Brillouin zone with small unfilled areas remaining in the first zone. As the electron concentration increases (corresponding to an increasing Te concentration) the Fermi surface expands until it contacts the boundary between the second and third Brillouin zones. Due to the energy gap across this boundary, the Fermi surface does not immediately break through into the third zone, but rather continues to expand in the second zone. When the Fermi energy becomes sufficiently large electrons begin to fill the third zone. This process is shown schematically in two dimensions in Fig. 24. Between the state shown in (a) of Fig. 24 and contact with the boundary, the area of the Fermi surface will expand. Somewhere between contact with the zone boundary, and the state shown in (b), the area of the Fermi surface will begin to contract, reflecting the fact that the second zone is filling up. When electrons begin to fill the third zone, the area of the Fermi surface should once again begin to increase. It is also expected

that the density of states will reflect these changes in the area of the Fermi surface. The electronic density of states is defined by

$$N(E) = \frac{1}{8\pi^3} \iint \frac{dS}{|\nabla_k E|} \tag{9}$$

where dS is an area element, and the integral is taken over the surface of constant energy E. For the largest part of most of the constant energy surfaces the result for $|\nabla_k E|$ is just the free electron expression

$$|\nabla_k E| = \frac{\hbar^2}{m} (k_x^2 + k_y^2 + k_z^2)^{\frac{1}{2}} = (\frac{2\hbar^2}{m} E)^{\frac{1}{2}} \tag{10}$$

Only in the immediate area of a Brillouin zone boundary does $|\nabla_k E|$ deviate significantly from this result. It is expected, then, that the density of states at the Fermi surface will increase until just after contact with the zone boundary, and will then decrease until electrons begin to fill the third zone. When this occurs $N(E)$ should once again begin to increase. This is actually a fairly old concept and was first proposed by Jones[20]. He predicted that whenever the Fermi surface contacts a Brillouin zone boundary, the electronic density of states should deviate from the free electron parabola, by showing first a maximum and then a minimum as energy increases. A similar result was proposed by Nutkins in 1956[21], with a very interesting but complicated geometrical method. His method, which he applied to the body centered cubic crystal structure, was to treat the system as though the electrons were entirely free,

and compute the density of states in each Brillouin zone as a function of energy. The total density of states, obtained by adding all the pieces at a given energy is just the free electron parabola. He then applies the very rough assumption that the curve for each zone can be shifted in energy by an amount due to the energy gap at the zone boundary. This is a somewhat crude method, but when the total density of states is calculated after the shift in energy, the curve, shown in Fig. 25, shows a maximum followed by a minimum in the region of the zone boundary. The results are expected to be similar, although not quite as pronounced, in the simple cubic case. This would be an interesting construction to do for the simple cubic crystal structure, but the geometrical complexity was sufficiently great that it was not undertaken.

Since the alloys dealt with in this study are disordered and do not possess a periodic potential in any strict sense, it seems in order to review the idea of band structure in a non-periodic potential. All the usual methods of band structure calculations (Nearly Free Electron, Augmented Plane Wave, Orthogonalized Plane Wave, Tight Binding, Pseudopotential) and even the concepts associated with $\bar{k}$ space depend on the use of Bloch waves and Bloch's theorm. Without going into details, Bloch's theorm states that the wave function of an electron in a perfect crystal may be expressed in the form[22]

$$\psi_k(\bar{r}) = e^{i\bar{k}\cdot\bar{r}} \; U_k(\bar{r}) \qquad (11)$$

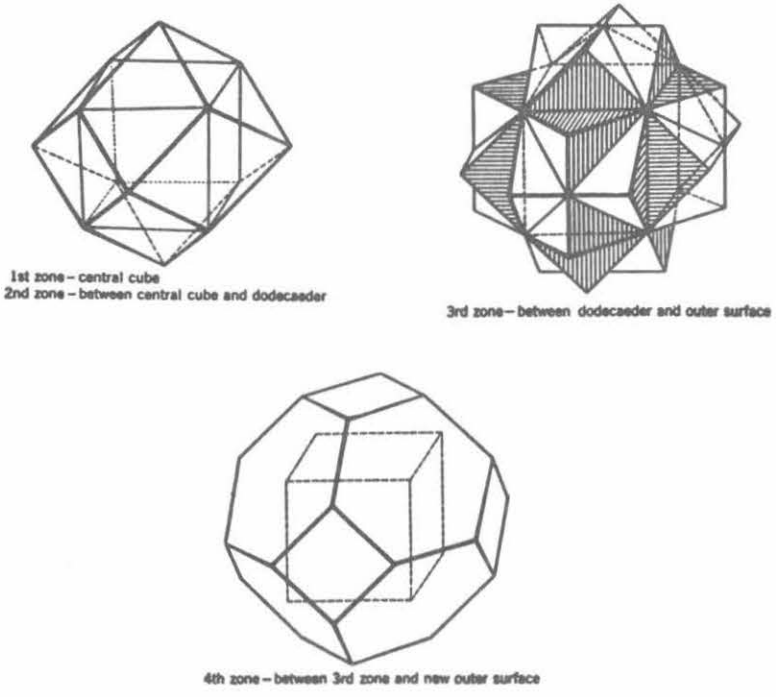

Fig. 23 Brillouin zones for the simple cubic crystal structure

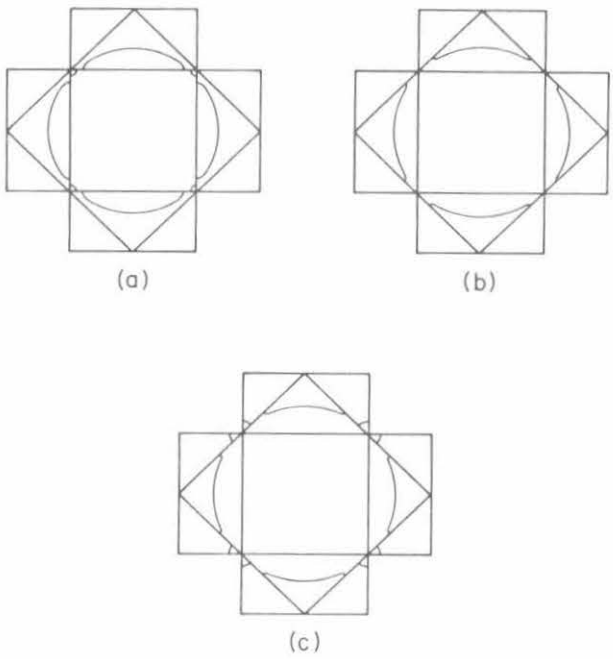

Fig. 24 Two-dimensional projection of the proposed Fermi surface in Te-Au alloys a)before contact with the second Brillouin zone boundary, b) after contact and c) as electrons fill the third zone

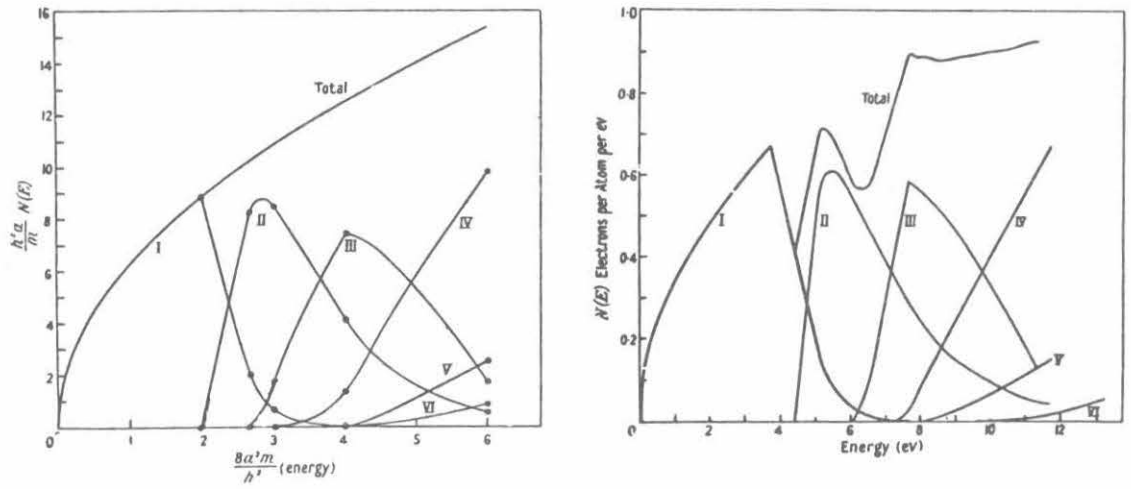

Fig. 25 Electronic density of states for the first 6 Brillouin zones of the bcc structure based on free electron calculations by Nutkins, with and without energy shifts between zones

where ψ_k is the electronic wave function, and $U_k(\bar{r})$ is a function which has the periodicity of the lattice. This formulation is consistent with the lattice since it produces an electronic density which has the same periodic properties as the lattice itself. Since in this formulation, the value of $\bar{k}$ is associated with the momentum of the electron, it provides a necessary and convienient way of cataloging a very large number of eigenfunctions, each of which describes two electrons throughout the entire crystal. One knows from the Pauli exclusion principle, and certain boundary conditions exactly how many electrons a certain region of $\bar{k}$ space can accomodate, hence it is possible to obtain a satisfactory picture of the band structure by solving for $E(\bar{k})$ for a relatively small number of $\bar{k}$ values. Were it not for Bloch's theorm it seems that it would probably be necessary to solve for each electronic wave function separately, which is an impossible task.

The theoretical basis for Bloch waves is the perfect periodicity of the crystal lattice. This is not an unreasonable assumption in a crystalline element, where an electron may travel many atomic distances before it encounters an imperfection (dislocation, interstitial atom, vacancy, etc) which disturbs the periodicity of the lattice. The presence of impurities, however, rapidly destroys the periodicity of the lattice. Not only is the potential at each lattice site not identical, but due to the size difference of the solute and solvent atoms, even the location of the lattice sites is no longer exactly periodic. The ultimate destruction of the periodicity is probably achieved in amorphous solids such as

those studied in Refs. 23, 24 and 25, where the arrangement of atoms is not only disordered, but there exists no crystal lattice at all. Bloch's theorm, and the concept of Bloch waves seem to have no theoretical basis under conditions such as these. However, work in disordered alloys[26] shows that in some cases the results of methods based on Bloch waves are capable of at least a qualitative explanation of experimental results. Work done on an amorphous semiconductor[24] has also shown that the qualitative aspects of the energy gap are not drastically different from those of crystalline semiconductors. In light of these facts one may be led to wonder how important long range ordering and the Bloch condition are to band structure theory.

Several theoretical attempts have been made to explain band structure in disordered[27] and amorphous alloys[28-31]. In the case of a disordered alloy attempts have been made to treat the difference between the potential of the solute atom and the potential of the solvent atom as a first order perturbation. Not enough work has been done using this method to indicate whether it produces results compatible with experimental work, but one might wonder if the difference in potential between two atoms whose atomic numbers may differ by 10 or 20 is really small enough to be treated as a perturbation. This method also makes no allowance for the disturbance caused by the size effect. In Ref. 29 Makinson and Roberts have developed a theoretical band structure for a one-dimensional amorphous material. Starting from a line of atoms arranged periodically they allowed the position of each atom to be determined by a pro-

bability distribution. The result of these calculations was a band structure very similar to that which is obtained for a periodic one-dimensional array. The major difference seems to be that the energy gap is not as sharp as in the crystalline case, the edges being somewhat diffuse. A brief summary of the theoretical work on amorphous alloys may be found in Ref. 24.

D. Electron Concentration

Before using the above model to interpret the experimental results which have been presented, a discussion of the electron concentration and its variations with alloying seems to be in order. The outer electronic configuration of the Au and Te atoms are $6s^1$ and $5s^2\ 5p^4$ respectively. The choice of a valence for Au seems quite unambiguous, so +1 electron per atom was chosen. Te, however, suggests two possibilities, +4 or +6 depending on whether or not one chooses to lump the two 5s electrons with the core states. Atomic structure calculations by Herman and Skillman[32] show that for isolated atoms, the 6s level in Au and the 5p levels in Te lie at about the same energy, while the 5s level of Te has a considerable lower energy. Since the energy levels for the isolated atom will be shifted somewhat when it is placed in a solid, it would be very dangerous to try to make any detailed statements about the band structure from this information. However, it does provide a qualitative basis for regarding the 5s electrons of Te as core electrons. With the above facts in mind, the remainder of this analysis treats Te as though it contributed four electrons per atom to the conduction bands. It should also be noted that the valence of each element

is assumed to be independent of alloying. That is, the electron per atom ratio varies from +1 to +4 linearly with composition. The conclusions resulting from this assumption are in satisfactory agreement with the experimental results.

The assignment of a valence for iron is somewhat more difficult. Its outer configuration is $3d^6\ 4s^2$, but this is not enough information to determine how it contributes to or removes electrons from the conduction band. The important factors in this determination are 1) whether or not Fe has a localized magnetic moment in Te-Au alloys, and 2) are the 4s electrons contributed to the conduction band. From the experimental results, and the discussion in chapter F of this section, it has been concluded that Fe has very little or no magnetic moment in the alloy system being studied. This immediately implies that conduction electrons from the Au and Te atoms have entirely filled the localized d-bands of the Fe atoms, requiring that for every Fe atom added to the alloy, 4 conduction electrons be removed from the Fermi sea. The disposition of the 4s electrons is much more difficult to ascertain, and in the absence of any specific theoretical or experimental evidence, their treatment will be somewhat arbitrary. Wilson, in Ref. 33, concludes that in some cases involving Fe and Co, the 4s electrons join the conduction band resulting in a valence of -2 for Fe. On the other hand, APW calculations for bcc Fe[62] show that the 4s band is well below the 3d band and does not even extend close to the Fermi surface. Unfortunately, there exists no evidence of what happens to the 4s band when Fe is dissolved in Te-Au, so the decision to assign a valence of -4 to Fe must be based on the

consistency in the resulting interpretation of the experimental results.

E. Thermoelectric Power of Au-Te

The thermoelectric power of metallic conductors consists of two parts, the first contribution from thermal diffusion of the conduction electrons and the second from phonon-drag. In the temperature range where the thermoelectric power is a linear function of temperature (i.e. $\sim 140^{\circ}K$ and higher) the phonon-drag contribution is probably not significant, so that only the diffusion term will be considered. Following this assumption, the thermoelectric power S(T) can be expressed as[34]

$$S(T) = -\frac{\pi^2 k^2 T}{3|e|}\left[\frac{\partial \ln\sigma(E)}{\partial E}\right]_{E=E_F} \tag{12}$$

where $\sigma(E)$ is the electrical conductivity associated with electrons of energy E. One may also write from elementary transport theory

$$\sigma(E) = \frac{e^2}{12\pi^3\hbar}\Lambda A_F \tag{13}$$

where Λ is the mean free electron path and A_F is the area of the Fermi surface. This leads to the following expression for thermoelectric power

$$S(T) = -\frac{\pi^2 k^2 T}{3|e|}\left[\frac{\partial}{\partial E}\ln\Lambda + \frac{\partial}{\partial E}\ln A_F\right]_{E=E_F} \tag{14}$$

The expression for $\sigma(E)$ used to derive this is strictly valid only if the mean free path is the same everywhere on the Fermi surface, a condition which is satisfied

only for completely free electrons. However, since the majority of the Fermi surface is spherical, it is expected that this approximation will yield reasonable accuracy.

In general, the Fermi energy varies very little with temperature[35], and consequently $\partial \ln A_F / \partial E$ is approximately temperature-independent. On the other hand it seems reasonable to assume that the electron mean free path is a function of temperature as well as energy. Therefore, the partial derivative $\partial \ln \Lambda / \partial E$ can be a function of energy and temperature, and may contain a constant arising from a linear energy term in the expression for the mean free path. To interpret the thermoelectric power data, it is necessary to further assume that the constant contained in the term $\partial \ln \Lambda / \partial E$ is negligible. The justification for this assumption is the agreement with the experimental results. Based on the assumptions just made, and as a first approximation, the following expressions are obtained:

$$\left[\frac{\partial \ln \Lambda}{\partial E}\right]_{E=E_F} = -\frac{3|e|}{\pi^2 k^2} \frac{1}{T} A \qquad (15)$$

$$\left[\frac{\partial \ln A_F}{\partial E}\right]_{E=E_F} = -\frac{3|e|}{\pi^2 k^2} B \qquad (16)$$

where A and B are the constants used in Eq. (1) of Section III, Chapter A. From Eq. (16) and Fig. 7, it can be inferred that the Fermi surface area increases with increasing Te content for alloys containing 60-73 at % Te. The rate of increase

of A_F is sharply reduced in the composition range 70-73 at % Te. It should be noted that $[\partial \ln A_F/\partial E]_{E=E_F}$ is positive for alloys with Te content less than 73 at %. At approximately 73 at % Te, $[\partial \ln A_F/\partial E]_{E=E_F}$ is zero and above this concentration it is negative. This last condition implies that the Fermi surface area starts to decrease with increasing Te content. This situation continues until 77 at % Te is reached, where the rate of decrease of A_F seems to be retarded. This effect reaches its maximum at about 80 at % Te, above which the rate of decrease of A_F is again more pronounced.

From the above analysis of the variation of $[\partial \ln A_F/\partial E]_{E=E_F}$ with concentration, it can be concluded that (a) for alloys containing 60-73 at % Te the area of the Fermi surface increases with Te concentration. This indirectly implies that the concentration of conduction electrons also increases with increasing Te content. (b) The Fermi surface touches the second Brillouin zone boundary at about 70 at % Te. Numerical calculations for completely free electrons in the second zone show that the area of the Fermi surface increases with increasing electron concentration until the Fermi surface is in contact with the zone boundary. After the contact, the Fermi surface area decreases with increasing electron concentration. In the case of nearly free electrons, it is expected that the transition from an increasing to a decreasing Fermi surface area will be smooth rather than discontinuous as in the free electron model. Thus, the point at which $[\partial \ln A_F/\partial E]_{E=E_F}$ shows a sharp decrease corresponds to the Fermi surface contacting the Brillouin zone. (c) The concentration variation

of $[\partial \ln A_F / \partial E]_{E=E_F}$ above 77 at % Te may be interpreted as the onset of the overlapping of the third band. The contribution of the second band to $[\partial \ln A_F / \partial E]_{E=E_F}$ is cancelled by the growth of the Fermi surface in the third band. Above 80 at % Te the experimental results of $[\partial \ln A_F / \partial E]_{E=E_F}$ reflect the competition between the two energy bands. At 85 at % Te, which is the limit of the simple cubic range, it seems that the second Brillouin zone still contains unfilled states.

The compositional dependence of the quantity $A(E_F)$ can be explained in two entirely unrelated manners. The dependence of $A(E_F)$ on composition can be used to obtain an approximate expression for the electron mean free path as a function of energy and temperature. From Eq. (15) it can be shown that

$$\ln \Lambda(E,T) = -\frac{3|e|}{\pi^2 k^2} \frac{1}{T} \int_0^E A(t)\, dt + f(T) \qquad (17)$$

where t is a variable of integration, and $f(t)$ is an undertermined function of temperature, the analytical form of which is not needed in the present discussion. The expression for the electron mean free path can be readily obtained from Eq. (17)

$$\Lambda(E,T) = e^{\left[\frac{L(E)}{T} + f(T)\right]} \qquad (18)$$

$$= F(T)\, e^{\frac{L(E)}{T}}$$

where

$$F(T) = e^{f(T)}$$

$$L(E) = - \frac{3\,|e|}{\pi^2 k^2} \int_0^E A(t)\, dt$$

In view of the approximations made in deriving the expression for the mean free path, it is expected to be useful only for a qualitative interpretation of physical properties such as resistivity.

An alternate explanation of the variation of $A(E_F)$ involves the possible presence of small amounts of amorphous material. A very similar alloy, $Au_5 - Cu_{25}Te_{70}$ studied by Tsuei[24] was found to be an amorphous semiconductor as mentioned earlier. Its thermoelectric power was reported as being very large ($\sim 300 \mu V$ per $^{\circ}C$) and with little temperature variation in the region being considered. It might be expected then that any amorphous Te-Au present would probably behave in a similar manner. Adding this contribution to the thermoelectric power one would expect 1 or 2% of amorphous material to have no effect on the slope of the thermoelectric power, but rather to contribute a substantial amount to the intercept value A. The variation of $A(E_F)$ then, may merely reflect the presence of amorphous material whose amount and properties are a function of composition and quenching rate. The experimental results of resistivity measurements suggest a preference for the second explanation, but are not conclusive enough to make any definite statement.

F. Superconducting Transition Temperature and its Relationship with Band Structure

The BCS theory of superconductivity[36], predicts that the zero field transition temperature from the normal to superconducting state depends on the product of the electronic density of states at the Fermi surface $N(E_F)$ and the strength of the attractive electron phonon interaction U, in the following manner,

$$T_C = 1.14\,\theta_D \exp\left[-1/N(E_F)U\right] \qquad (19)$$

where θ_D is the Debye temperature. The compositional variation of the superconducting transition temperature shown in Fig. 11 is believed to reflect the variation of the product $N(E_F)\ U$ with alloying. If one assumes that the electron phonon interaction potential changes monotonically with composition, then the curve in Fig. 11 should be qualitatively the same as the electronic density of states at the Fermi surface. Although it is difficult to make any conclusive statements about either $N(E_F)$ or U separately without information such as electronic specific heat, the agreement between the proposed model and the observed transition temperature variation seems to support the above assumption.

According to Havinga[37], when the Fermi surface is approaching or intersecting a Brillouin zone, the electron phonon interaction is increased, thereby enhancing the superconducting transition temperature. The Fermi surface-Brillouin zone interaction may then serve to explain the unusual occurrance of

superconductivity in this alloy system.

1. Band Structure Effect in Te-Au-Fe Alloys

As pointed out previously, Fe added to Te-Au alloys behaves as though it had a valence of approximately -4. This implies that the addition of small amounts of Fe will cause the Fermi surface to move relatively large distances in momentum space. Therefore, before the impurity effect of Fe on the transition temperature can be determined, it is necessary to correct somehow for the change in the superconducting transition temperature due to the changing position of the Fermi surface. Allowing the following assumptions, it is possible to separate these two effects on the basis of the model presented using the information obtained concerning the superconducting transition in Te-Au. It must be assumed that (1) compositional dependence of the transition temperature of pure Te-Au is due entirely to a changing Fermi surface within a rigid band model, and (2) that the addition of 2-3 at % Fe does not significantly alter the band structure. Based on these assumptions then, the following correction proceedure is used. The concentration of electrons per atom is computed for the Te-Au-Fe alloy being corrected. The composition of the Te-Au alloy which has the same electronic concentration is then determined, and the superconducting transition temperature of this alloy is read from Fig. 11. This temperature, T_{C1}, is the transition temperature one would expect the Te-Au-Fe alloy to exhibit if the addition of Fe had no effect other than to change the location of the Fermi surface. The actual observed transition temperature of the Te-Au-Fe alloys, T_{C2}, was in all cases

lower than T_{C1} . This implies that either disordering or magnetic properties of the Fe lowered the superconducting transition temperature by an amount $\Delta T = T_{C1} - T_{C2}$. The corrected transition temperatures shown in Figs. 26, 27, 28, are given by the formula

$$T_C(n) = T_{C0} - \Delta T(n) \qquad (20)$$

where T_{C0} is the transition temperature of the host alloy to which Fe is being added, and n is the Fe concentration. This correction is obtained for each alloy as follows. The alloy $(Te_{75}Au_{25})_{98.5}Fe_{1.5}$, for example, becomes superconducting at 2.25°K (Fig. 14). The electron per atom ratio for this alloy computed on the basis of Au = +1, Te = +4, and Fe = -4, is 3.14 electrons per atom. In the binary Te-Au system, this ratio corresponds to the alloy $Te_{71.3}Au_{28.7}$. From Fig. 11, the transition temperature of this alloy is found to be 2.95°K, hence, the impurity effect of the Fe is to lower the transition temperature by an amount $\Delta T = 2.95 - 2.25 = 0.70°$ K . The transition temperature of the host alloy, $Te_{75}Au_{25}$ is 2.66°K (Fig. 14). Therefore, the corrected transition temperature for this alloy is given by $T_c = T_{co} - \Delta T = 2.66 - 0.70 = 1.96°K$.

2. Localization of the Magnetic Moment in Te-Au-Fe and Te-Au-Mn Alloys

Since the presence or absence of a localized magnetic moment determines the compositional variation of the superconducting transition temperature in the

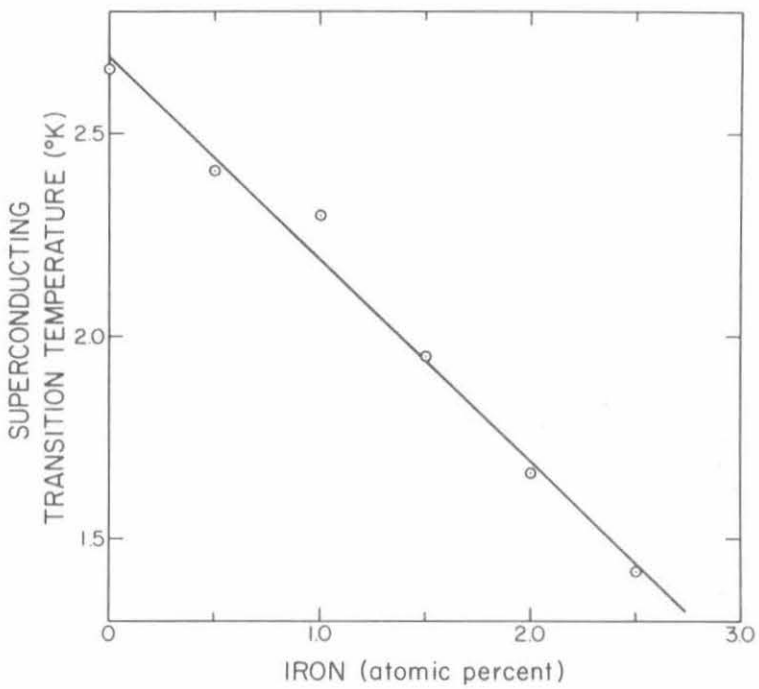

Fig. 26 Superconducting transition temperature of simple cubic alloys $(Te_{75}Au_{25})_{100-x}Fe_x$ after correction described in Eq. (20)

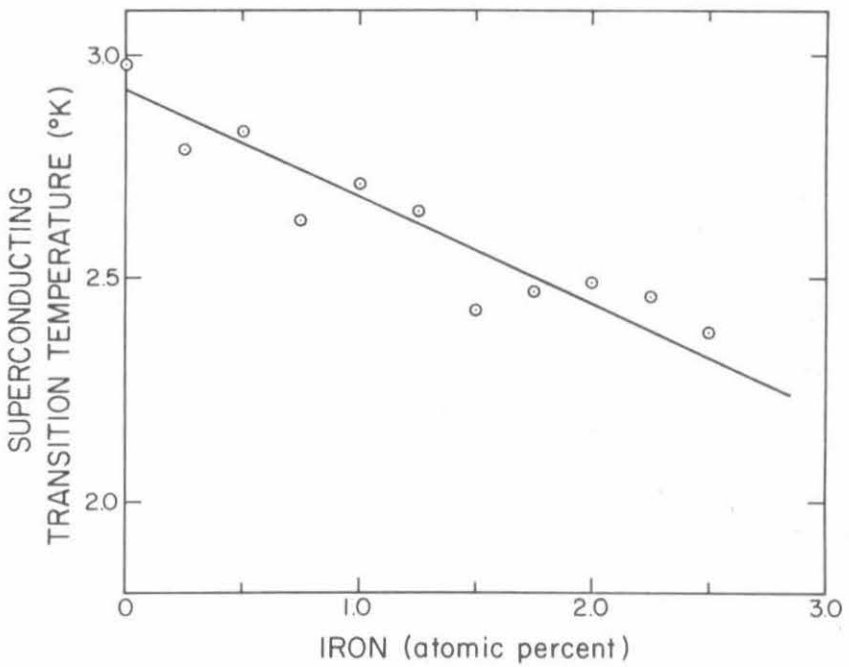

Fig. 27 Superconducting transition temperature of the simple cubic alloys $(Te_{70}Au_{30})_{100-x}Fe_x$ after correction described in Eq. (20)

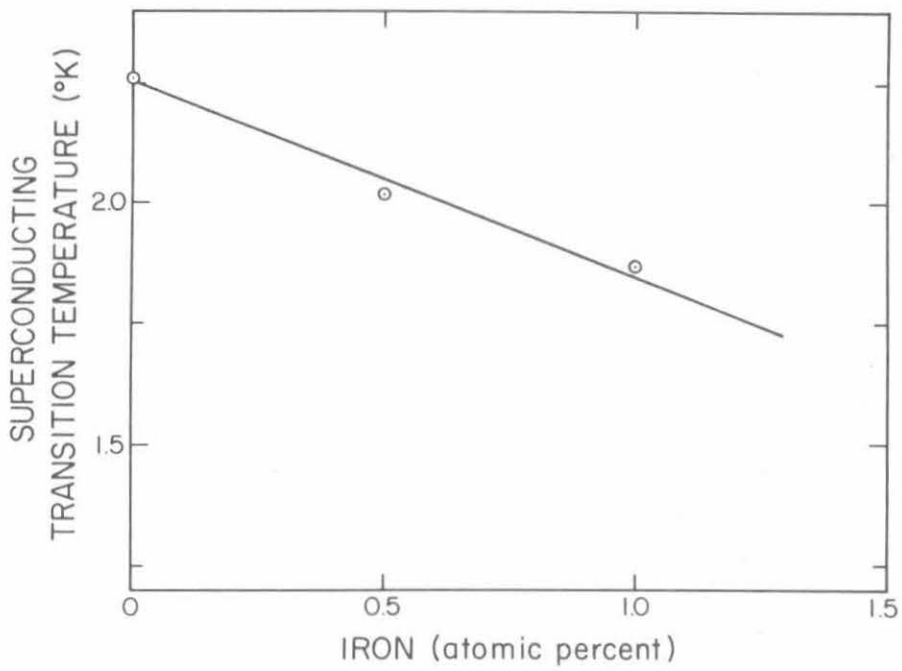

Fig. 28 Superconducting transition temperature of the simple cubic alloys $(Te_{65}Au_{35})_{100-x}Fe_x$ after correction described in Eq. (20)

Te-Au-Fe system it will be discussed along with the transition temperature results. The basic qualitative argument concerning the formation of a localized moment is due primarily to Friedel[20]. He argues that when an element of the first transition series is added to a solute, the 3d energy levels of the impurity resonate with the conduction states of the solute. This causes a broadening of the 3d band of the impurity, and a relative shift between the $3d\uparrow$ band and the $3d\downarrow$ band. If the Fermi level of the host lies entirely above or entirely below the impurity levels, then both the $3d\uparrow$ and the $3d\downarrow$ bands will be completely full or empty, and the impurity will exhibit no localized moment. If, however, the Fermi level falls in the region of the impurity levels, then due to the shift between bands of opposite spin, there will be unequal numbers of $3d\uparrow$ and $3d\downarrow$ electrons, and the impurity will exhibit a localized moment. This effect is illustrated in Fig. 29.

From information tabulated in Ref. 38, it is clear that for Fe, the top of the 3d bands seems to fall just above 7 ev, and for Mn somewhere between 10 and 12 ev. Using the following formula for free electrons,

$$E_F = \frac{\hbar^2}{2m} (3\pi^2 \frac{N}{V})^{\frac{2}{3}} \qquad (21)$$

where E_F is the Fermi energy, N is the number of electrons per atom, and V is the atomic volume, to get a rough idea of the Fermi energy in the Te-Au system, it is found to vary from 8.4 ev to 8.9 ev for $Te_{60}Au_{40}$ and $Te_{85}Au_{15}$ respectively. On the basis of this information and Friedels model, one would expect that Fe dissolved in Te-Au would not have a localized magnetic moment, but Mn dissolved

in the same alloy system would. Measurements of the low temperature magnetoresistance reported in Chapter D of Section III seem to support this conclusion. The alloy $(Te_{70}Au_{30})_{98.5}Mn_{1.5}$ shows a negative magnetoresistance as would be expected if a localized moment were present on the Mn atom, while the alloy $(Te_{70}Au_{30})_{98.5}Fe_{1.5}$ exhibits a positive magnetoresistance, consistent with the absence of a magnetic moment. The most direct evidence to confirm or refute the presence of a magnetic moment would be susceptability measurements. Due to the small amount of alloy obtained from a single quench and the low percentages of magnetic impurity in the alloy, the number of quenches required to make such a measurement is forbiddingly large. It would indeed be interesting, however, to determine which of the alloys show Curie-Weiss behavior.

Since direct evidence is not obtainable the existence of a magnetic moment must be inferred from other measurements. As shown in Table IV, the effect of the impurity on the superconducting transition temperature can yield a great deal of information concerning the existence of a localized moment. It can be seen that the suppression of the transition temperature of a given host lattice is increased by at least an order of magnitude when the impurity has a localized moment. Data for the alloys $(Te_{70}Au_{30})_{100-x}Fe_x$ and $(Te_{70}Au_{30})_{100-x}Mn_x$ show that dT_c/dc, where T_c is the superconducting transition temperature, and c is the concentration of magnetic impurity, is at least 10 times larger for Mn than for Fe. This evidence provides further support for the conclusion drawn from Friedel's model.

TABLE IV

Effect of the transition metals on the superconducting transition temperatures of various hosts.

Alloy System	dT_c/dc (°K/at% x)	Magnetic moment
$Zn_{100-x}Cr_x$	-180 (56)	Yes (61)
$Zn_{100-x}Mn_x$	-310 (56) -170 (42)	Yes (59, 60)
$Zn_{100-x}Fe_x$	-13 (56)	Unknown
$Zn_{100-x}Co_x$	-6.4 (56)	Unknown
$Zn_{100-x}Ni_x$	-2.9 (56)	Unknown
$Al_{100-x}Cr_x$	-2.7 (42)	No (61)
$Al_{100-x}Mn_x$	-7.3 (42)	No (57, 58)
$Al_{100-x}Fe_x$	-2.4 (42)	No (57, 58)
$In_{100-x}Mn_x$	-6 (43)	No (43)

(The numbers in parenthesis refer to references)

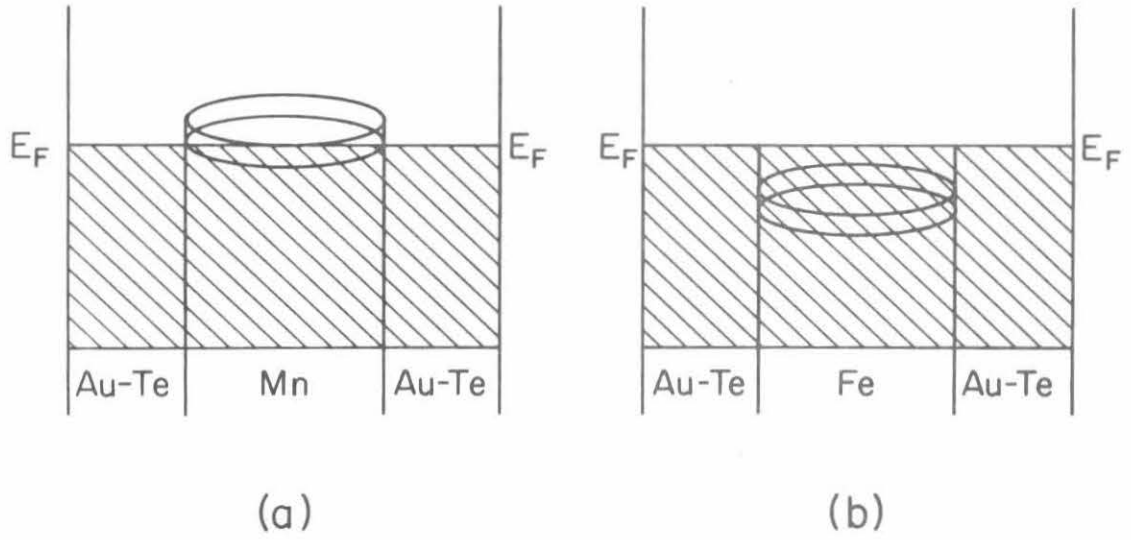

Fig. 29 Localized d-states for the simple cubic alloys a) Te-Au-Mn, and b) Te-Au-Fe, after Friedels model

3. Impurity Effect in Te-Au-Fe Alloys

In explaining the linearity of the T_c versus c, two possibilities must be considered. The first possibility is that the upper limit of the 3d band is not as sharp as Fig. 29 implies, but rather has something like a tail extending to higher energies. If the Fermi surface passes through this region a small number of 3d states would lie above the Fermi energy, and hence, would be unfilled. This would have essentially no effect on the assumed valence of Fe, but the very small magnetic moment which would result could effect the superconducting transition temperature. The other possibility is the complete absence of any localized moment, in which case the shape of the transition temperature curve must be explained entirely in terms of an impurity effect.

A rather complete theory to explain the effect of localized magnetic moment on the superconducting transition temperature has been proposed by Abrikosov and Gorkov[39]. While the details of their treatment are beyond the scope of this writing the results they obtain with the method of Green's functions are rather explicit and can be applied directly to experiments. Their general result is expressed in the form

$$\ln \frac{T_{C0}}{T_C} = \psi(\tfrac{1}{2}+\frac{\rho}{2}) - \psi(\tfrac{1}{2}) \qquad (22)$$

where

$$\rho = \frac{1}{\pi \tau_s T_C}$$

and

$$\frac{1}{\tau_s} = \frac{n m \rho_o}{2\pi^2} \frac{s(s+1)}{(2s+1)^2} \int |f_+ - f_-|^2 \, d\Omega$$

where n is the impurity concentration, m is the mass of an electron, ρ_o is the momentum transfer, s is the spin of the impurity, f_+ and f_- are electron scattering amplitudes and ψ is the digamma function. For the impurity concentration ranges in the Te-Au-Fe alloy system the formula can be put in the more explicit form

$$T_C = T_{C0} - \pi/4 \tau_s \tag{23}$$

Substituting the expression for τ_s shown by Parks[40] we finally obtain

$$T_C = T_{C0} - \frac{1}{8} n \pi N(E_F) \; J^2_{ex} \; s(s+1) \tag{24}$$

where $N(E_F)$ is the density of states at the Fermi surface, and J_{ex} is the strength of the exchange scattering from the impurities. If the variations of $N(E_F)$ and J_{ex} are only a few percent over the range of impurity concentration, then Eq. (24) predicts that T_c will decrease linearly with increasing Fe concentration. This result is indeed consistent with the corrected experimental data.

The second possibility presented assumes that the Fe has no magnetic moment at all when dissolved in Te-Au alloys. If this is the case then the only effect on the transition temperature should be an impurity effect, and the theory of Markowitz and Kadanoff[41] should be of value in explaining the shape of T_C versus c. The main conclusion of this theory is the prediction that the transition temperature should be of the following form,

$$T_C = T_{C0} - K^i X - \langle a^2 \rangle T_C I_C(X) \qquad (25)$$

where K^i is a constant depending on the host, X is a variable proportional to concentration, $\langle a^2 \rangle$ is a factor which depends on the anisotropy of the electron phonon pairing potential and $I_C(X)$ is a fairly complicated integral which is of no interest in this discussion. According to the authors, the term $\langle a^2 \rangle T_C I_C(X)$ is due to the reduction in anisotropy resulting from a reduction in the mean collision time, and the linear term $K^i X$ is due to a change in the gross properties of the system. The above formula was developed for the addition of an impurity to an elemental superconductor. In such a case, small amounts of impurity will greatly reduce the mean collision time and smooth out the anisotropy of the pairing potential. In the case being considered here, the host material is already a completely disordered solid solution, and it seems unlikely that the addition of a few iron atoms will have much effect at all on the mean collision time. Hence, the last term in Eq. (25) may be disregarded entirely and it reduces to the form

$$T_C = T_{C0} - K^i \lambda c \qquad (26)$$

where λ is the proportionality constant between x and c. This formula describes the same kind of variation as Eq. (24) which resulted from the AG theory, and consequently also describes the experimental results. It should be realized in evaluating this explanation that (1) the theory was developed using an elemental and not a solid solution host, with the result that some of the parameters, such as mean collision time, will not vary in the manner assumed, and (2) the theory was intended to apply to cases where the transition temperature was altered by a few percent, and not by the larger amount occurring in the present alloy systems.

In the case of elemental superconductors it should be possible to differentiate between mechanisms, since they predict different concentration dependances of T_c. An examination of the shapes of the T_c versus c curves for several alloy systems where the host material is an elemental superconductor and the solute is a metal from the first transition series (without a detectable localized moment) seems to support the second explanation. The systems Al - Cr and Al - Mn[42] seem to show a definite curvature of the type predicted by Markowitz and Kadonoff. The work by Martin[43] on the system In-Mn also suggests this same mechanism although the amount of Mn in solid solution may be open to questions as a result of the technique of alloy preparation. The work of Opitz[44] on the system In-Fe shows a linear relationship between Tc and Fe concentration very similar to that observed in this study. His samples were prepared by vapor deposition which results in a very fast quench, probably

introducing many imperfections (vacancies, interstitials, dislocations, etc) into the crystal structure. This is likely to have the same effect as disordering in an alloy, since it will reduce the mean free path and probably smooth out the anisotropy in the electron pairing potential. If this is the case, then a linear relationship such as that observed is consistent with this interpretation of the theory of Markowitz and Kadonoff.

G. Lattice Parameter and Band Structure

From the experimental evidence presented, and the discussion above, it seems fairly conclusive that a Fermi surface-Brillouin zone interaction of some sort is taking place in the alloy system studied. It is appropriate, then, to give some consideration to the effect this interaction may have on the lattice parameter. It has been strongly suspected for almost 40 years that electron concentration and Brillouin zones are among the factors influencing crystal structure type and lattice spacing[45]. Jones (1935) achieved good qualitative success in explaining Hume-Rothery's electron compounds[46] in terms of a peak in the density of states versus energy curve in the region of a Brillouin zone boundary. He also achieved apparent success in explaining lattice parameter anomalies in the system Mg-Cd as an interaction between conduction electrons and the Brillouin zones. Since that time, a number of authors have studied this problem both experimentally and theoretically with rather conflicting results. It is hoped that the work presented here will clarify to some extent the experimental aspects of this problem. Before considering the Te-Au system it is felt

that a short discussion of the relationship between lattice parameter and band structure and some of the prominent theories is in order.

1. Theories of Jones and Goodenough

The first attempt to show a relationship between Fermi surface-Brillouin zone interactions and the lattice spacings of a solid was a theory presented by Jones[47,48]. To consider the effect of electrons on the high energy side of a Brillouin zone boundary, he presented a development which can be summarized as follows. If one considers those electrons contained between a Brillouin zone boundary and the Fermi surface, their total energy per atom may be written as

$$U = 2\tau \int E(\bar{k})\, dV \tag{27}$$

where τ is the atomic volume, $\bar{k}$ is the momentum wavevector of the electron, dV is an element of volume in $\bar{k}$ space, and the integration is carried out over the volume between the Brillouin zone and the Fermi surface. If the crystal is now strained in a direction perpendicular to the Brillouin zone boundary being considered, the total energy per atom, U, will change in the following manner,

$$\frac{\partial U}{\partial \epsilon} = 2\tau \int \frac{\partial E}{\partial \epsilon}\, dV \tag{28}$$

Eq. (28) is based on the following assumptions: (1) the number of electrons contained between the Fermi surface and the Brillouin zone is constant under the strain, (2) the strain does not affect the value of the energy gap at the Brillouin zone boundary, (3) the atomic volume, and therefore the related volume

of the Brillouin zone in reciprocal space remains constant under the strain. This third assumption is not pointed out explicitly by Jones, but is very important in the following discussion. If σ is the stress which produces ϵ, then we may write

$$\tau\sigma = -n\overline{\frac{\partial E}{\partial \epsilon}} \tag{29}$$

where $\overline{\frac{\partial E}{\partial \epsilon}}$ is the average value of $\frac{\partial E}{\partial \epsilon}$ for the electrons being considered. Using the free electron result for $\frac{\partial E}{\partial \epsilon}$ Jones comes to the conclusion that electrons above a Brillouin zone boundary produce a stress perpendicular to that boundary which tends to expand the lattice. This stress is given by

$$\sigma = \frac{2n}{\tau}\bar{E} \tag{30}$$

where $\bar{E}$ is the average energy of the electrons being considered. This theory predicts that the lattice should show an anomalous expansion proportional to the number of electrons contained in the higher zone.

The important point to make concerning this theory, is that although it has some success in explaining lattice parameter anomalies in a number of non-cubic systems, particularly hexagonal,[49-51] it breaks down in the case of a cubic system. This occurs because the restriction that τ remain constant under the strain ϵ requires the ϵ be pure distortional strain. In a cubic material there is no way to apply a distortional strain without destroying the cubic symmetry, hence the restriction on τ cannot be met.

The next development, which served almost as an expansion of Jones theory was Goodenough's attempt to explain why some alloys show anomalous behavior of the lattice parameter before the Fermi surface contacts the Brillouin zone[52]. Goodenough's theory is based on the condition described earlier that surfaces of constant energy in momentum space must meet the Brillouin zone boundary perpendicularly. If one considers the E(k) curve for the nearly free electron model in one dimension it is clear that if the Brillouin zone is moved in slightly, corresponding to an expansion of the lattice, the E(k) contour must be bent to a slightly lower energy in order to satisfy the above mentioned criterion. This implies that if the Fermi surface is close to the Brillouin zone the total energy of the conduction electrons will be lowered slightly by this change in lattice spacing. Figures 30a and 30b illustrate this effect in one and two dimensions respectively. It is important to realize that when the Brillouin zone boundary is moved in, the scaling in $\bar{k}$ space is not changed, but rather the volume chopped off is merely transferred elsewhere. This mechanism predicts an anomalous expansion of the lattice as the Fermi surface approaches a Brillouin zone boundary. The major drawback of this theory, one which Goodenough himself mentions, is its inapplicability to cubic systems. From boundary conditions we know that a Brillouin zone will hold exactly $2N$ electrons, where N is the number of atoms in the crystal. If a given number of states are removed from the edge of one Brillouin zone boundary when it is moved in, they must be replaced in another part of the zone, since the volume

occupied by the zone in $\bar{k}$ space must remain constant in order to satisfy the above mentioned boundary conditions. What this amounts to is the same assumption made in Jones theory, i.e. that $\mathcal{T}$ must be constant under the deformation. Goodenough points out that in the cubic case, all the first order effects of his theory vanish.

1. Lattice Parameter Anomalies in Te-Au and Te-Au-Fe

It was pointed out in Chap. C of Section III that the variation of lattice spacing with composition for the Te-Au system shows an anomalous change of slope in the region of 67-68 at% Te. The lattice spacing on either side of this composition seems to vary quite linearly with composition. Calculations for the simple cubic Brillouin zone construction based on free electrons show that the Fermi surface contacts the second Brillouin zone boundary at an electron concentration of 2.96 electrons per atom. A calculation based on the valences previously discussed for Te and Au shows that the lattice parameter anomaly occurs at an electron concentration of approximately 3.0 electrons per atom. On this basis alone, it seems likely that the change in slope of the lattice parameter may be due to contact of the Fermi surface with the second Brillouin zone boundary. The main drawback to this argument is the existence of the equilibrium compound $AuTe_2$ at 66.7 at% Te. The experimental measurements of lattice spacings in the Te-Au-Fe system are necessary to show conclusively that this anomaly is due to the effect of conduction electrons and nothing else. In Fig. 31 the lattice spacings of $(Te_{80}Au_{20})_{100-x}Fe_x$, $(Te_{75}Au_{25})_{100-x}Fe_x$, $(Te_{70}Au_{30})_{100-x}Fe_x$, and

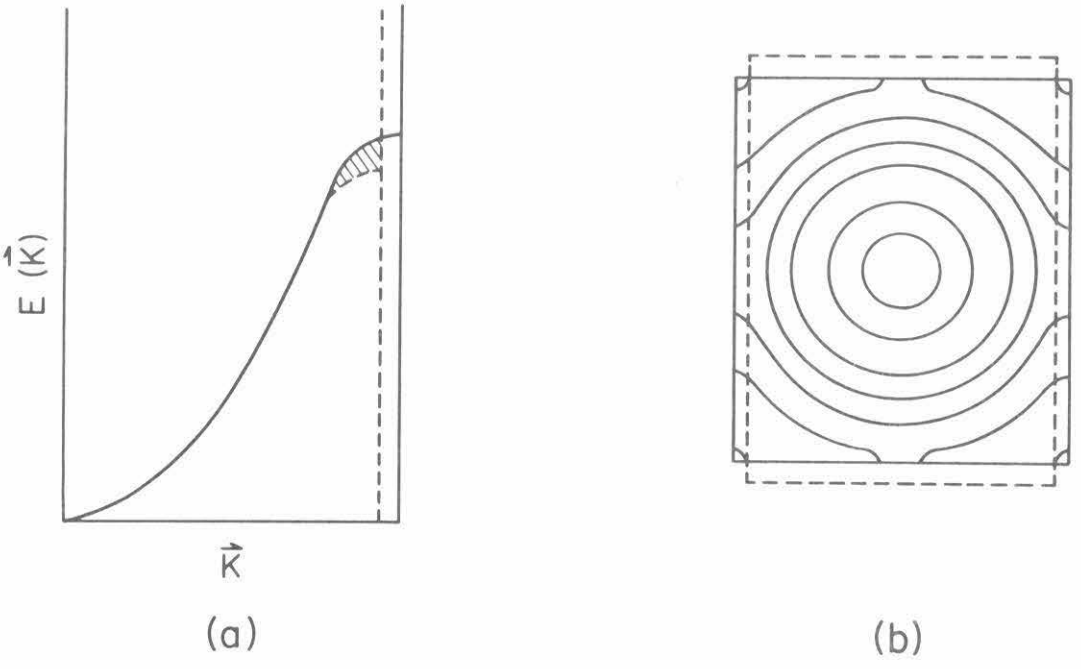

Fig. 30 a) E(k) for nearly free electrons, showing the effect of expanding the lattice. The shaded region represents energy saved by moving the Brillouin zone boundary. b) The dotted lines show the distortion of the first Brillouin zone described by Goodenough

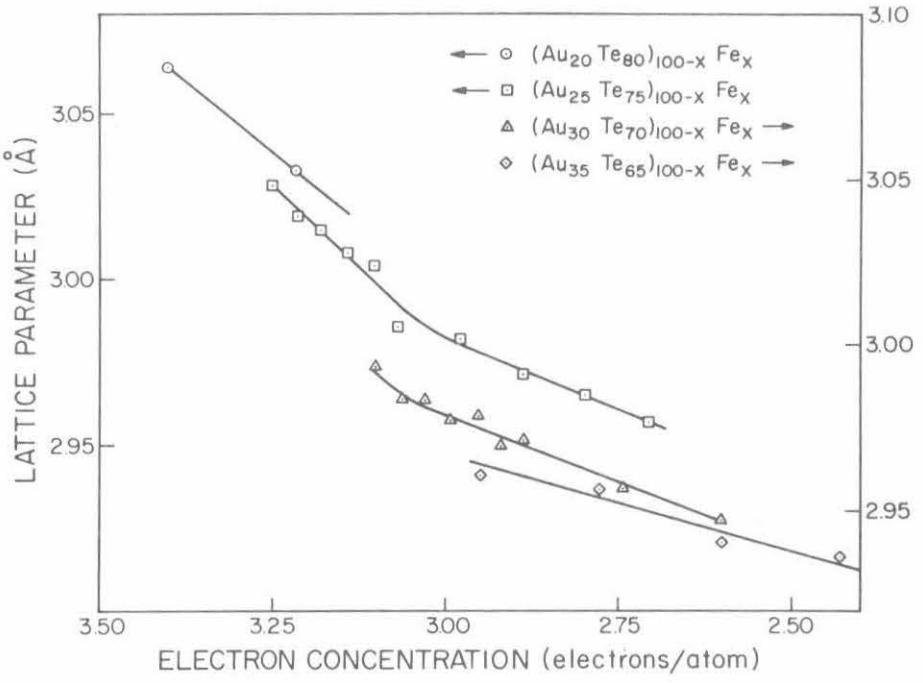

Fig. 31 Lattice parameter of the simple cubic Te-Au-Fe alloy as a function of electron per atom ratio

$(Te_{65}Au_{35})_{100-x}Fe_x$ are plotted versus electron concentration. It is clear from this figure that the slope of the lattice parameter changes at a point which is determined only by the electron concentration, and not by the composition of the alloy. Thus the anomalous behavior of the lattice parameter is an effect caused by the conduction electrons.

3. The System Li-Mg

The only example found of a lattice parameter anomaly which may be connected with a Fermi surface-Brillouin zone interaction in a cubic material is the Li-Mg solid solution. The work of Levinson[53] who studied alloys containing from 30 to 100 at% Li shows a very sharp minimum in the variation of lattice parameter with concentration of Li at ~50 at% Li. The data on both sides of this minimum seem to fall on linear segments. The data of Herbstein and Averbach[54] show a similar effect, though less pronounced and centered between 60 and 65 at% Li. Assigning Li and Mg valences of +1 and +2 respectively the minimum would occur between 1.4 and 1.5 electrons per atom. For the bcc structure, calculations based on free electrons show that the Fermi surface contacts the first Brillouin zone boundary at 1.48 electrons per atom. Thus, the lattice parameter anomaly occurs in a region of electron concentration consistent with a Fermi surface-Brillouin zone contact. The Li-Mg issue may be clouded however, by the possibility of CsCl ordering, which many bcc structures undergo in the region of $A_{50}B_{50}$, although there is no direct evidence available that such ordering actually does occur.[55]

From the above discussion, the following conclusions may be drawn: (1) The lattice parameter anomaly is a general phenomonon, in the sense that it can occur regardless of the type of crystal structure. (2) The lattice parameter of an alloy is affected by a balance between the electronic energy (including any contribution due to a Fermi surface-Brillouin zone interaction) and other terms such as correlation and exchange energies. In order to determine the effect on the lattice parameter of the Fermi surface-Brillouin zone interaction, a detailed knowledge of the band structure is probably required.

V SUMMARY AND CONCLUSIONS

The experimental findings of this study may be summarized as follows: (1) The superconducting transition temperature of the Te-Au alloys shows a maximum and a minimum at 70 and 80 at% Te respectively. (2) Measurement of the thermoelectric power of the Te-Au alloys shows unusual behavior in the regions of 70 and 80 at% Te. (3) The rate of change of lattice spacing with composition shows a distinct break around 67 at% Te. (4) The rate of change of lattice spacing with Fe concentration in $(Te_{75}Au_{25})_{100-x}Fe_x$ alloys shows a distinct break at about 3 at% Fe. (5) The superconducting transition temperatures of the Te-Au-Fe alloys decrease nonlinearly with the addition of Fe, and the effect of Fe is much smaller than might be expected. (6) The addition of Mn to $Te_{70}Au_{30}$ causes a very rapid depression of the superconducting transition temperature. (7) Magnetoresistance measurements show that Fe added to $Te_{70}Au_{30}$ causes a positive magnetoresistance, while Mn added to the same alloy produces a negative magnetoresistance. (8) Resistivity measurements performed on the alloy $Te_{66.7}Au_{33.3}$ show substantially linear temperature dependence.

From the experimental findings, and from the analysis of these results in section IV, several important conclusions may be drawn. The first, and probably most basic conclusion, is the existence of an interaction between the Fermi surface and a Brillouin zone boundary which has a marked effect on the bulk transport properties. It has been further demonstrated that the qualitative aspects

of the topology of the Fermi surface may be deduced from the interpretation of these transport properties. Second, the success of NFET in explaining the transport properties tends to confirm the validity of applying a theory based on Bloch waves and the perfect periodicity of the electronic potential to a solid whose electronic periodicity is strongly disturbed. The theoretical implications of conclusions of this nature may ultimately have an important effect on band structure calculations. Third, the successful splitting of the superconducting transition temperatures of the Te-Au-Fe alloys demonstrates that information about the electronic density of states, acquired from studying Te-Au alloys, may be used to separate the effect of Fe as an impurity from its effect on the band structure when added to Te-Au alloys. The fourth conclusion, regarding the anomalous behavior of the lattice parameter, is relevant to the theoretical study of the influence of conduction electrons on lattice spacings. It has been conclusively demonstrated in this work that a lattice parameter anomaly of the type occurring in many hexagonal alloys can occur in a cubic alloy. It has been further shown that this effect depends only on the concentration of conduction electrons and not on the alloy composition. Considering the large amount of independent evidence showing that the Fermi surface contacts a Brillouin zone boundary as this lattice parameter anomaly occurs, the conclusion that the lattice spacings are influenced by this contact is strongly supported.

Although the author attempted to make a thorough study of the alloys, several topics which are likely to yield interesting results were not investigated.

The transverse magnetoresistance of metallic alloys depends to some degree on the manner in which electrons may circulate on the Fermi surface. The motion of electrons on the Fermi surface depends in turn on how the surface connects to itself, i.e. whether it is closed or open. Since this is determined largely by the Brillouin zone boundaries, it is expected that the compositional variation of magnetoresistance in the Te-Au alloys will show a strong change in the region of contact with a boundary. The addition of elements from the first transition series other than Mn or Fe would provide additional information regarding the interpretations of localized magnetic moment, superconducting transition temperature, and lattice spacing discussed in this study. If the analysis applied in this work is correct, then Co and Ni dissolved in Te-Au should behave with valences of -3 and -2 respectively, and should not exhibit localized magnetic moments. The behavior of the superconducting transition temperature and the lattice spacings should reflect this shift in valence.

The work presented in this paper also adds interest to two theoretical problems being considered by several workers. The first problem is the calculation of energy band structure for electrons in a nonperiodic potential. The rising importance of this has already been pointed out, and it is hoped that this work will provide some useful experimental information along this line of study. The second problem, which is much more specialized, is the development of a new mechanism to explain the influence of conduction electrons and Brillouin zones on the lattice spacings of alloys. The inadequacies of the currently accepted

theories have been pointed out previously, and the results of this work should leave no doubt that a new explanation is required.

REFERENCES

1. W.H. Beamer and L.R. Maxwell, J. Chem. Phys. 17, 1293 (1964).
2. H.L. Luo and W. Klement, J. Chem. Phys. 36, 1870 (1962).
3. B.C. Giessen, U. Wolff, and N.J. Grant, Trans. AIME 242, 597 (1968).
4. C. Borromee-Gautier, B.C. Giessen, and N.J. Grant, J. Chem Phys. 48, 1905 (1968).
5. Pol Duwez and R.H. Willens, Trans. AIME 227, 362 (1962).
6. Pol Duwez, Trans. ASM 60, 607 (1967).
7. H. von Dijk, M. Durieux, J.R. Clement, and J.K. Logan, Natl. Bur. Std. (U.S.) Monograph 10, Part 2 (1960).
8. J.A. Schmitz and D.R. Ford, Rev. Sci.Inst. 37, 640 (1966).
9. The superconducting transition temperature of the simple cubic alloy $Te_{62.5}Au_{37.5}$ was reported by H.L. Luo, M.F. Merriam, and D.C. Hamilton, Science 145, 581 (1964).
10. M. Hansen, Constitution of Binary Alloys (McGraw-Hill Book Company, Inc., New York, 1958), p. 235.
11. G. Tunell and C.J. Ksanda, J. Wash. Acad. Sci. 25, 32 (1935).
12. Leon Brillouin, Wave Propogation in Periodic Structure (Dover Publications, Inc., New York, 1946), 2nd ed., p. 136.
13. C. Kittel, Introduction to Solid State Physics (Wiley-Interscience, Inc., New York, 1956), p. 268.

14. See Ref. 12, p. 152.

15. A.H. Wilson, The Theory of Metals (Cambridge at the University Press, London, 1936), 2nd ed., p. 34.

16. N.F. Mott and H. Jones, The Theory of the Properties of Metals and Alloys (Dover Publications, Inc., New York, 1936), p. 59.

17. See Ref. 12, p. 107.

18. See Ref. 13, p. 255.

19. W.A. Harrison, Pseudopotentials in the Theory of Metals (W.A. Benjamin, Inc., New York, 1966).

20. J. Friedel, Nuovo Cimento, 7, 287 (1958).

21. M.A.E. Nutkins, Proc. Phys. Soc., 69B, 619 (1956).

22. F. Bloch, Z. Physik 52, 555 (1928).

23. Pol Duwez, R.H. Willens, and R.C. Crewdson, J. Appl. Phys. 36, 2267 (1965).

24. C.C. Tsuei, Phys. Rev. 170, 775 (1968).

25. S.C.H. Lin and P. Duwez, Phys. Stat. Sol. 34, 469 (1969).

26. C.C. Tsuei and L.R. Newkirk, Phys. Rev. 183, 619 (1969).

27. N.F. Mott, Adv. Phys. 16, 49 (1967).

28. A.I. Gubanov, Quantum Electron Theory of Amorphous Conductors (Consultants Bureau Enterprises, Inc., New York, 1965).

29. R.E.B. Makinson and A.P. Roberts, Australian J. Phys. 13, 437 (1960).

30. R.E. Borland, Proc. Phys. Soc. (London) 78, 926 (1961).

31. Kazno Hiroike, Phys. Rev. 138, A422 (1965).

32. F. Herman and S. Skillman, Atomic Structure Calculations (Prentice-Hall, Inc., Englewood Cliffs, N.J., 1963).

33. See Ref. 15, p. 109

34. J.M. Ziman, Electrons and Phonons (Oxford University Press, New York, 1960), p. 397.

35. J.M. Ziman, Principles of the Theory of Solids (Cambridge University Press, Cambridge, 1964), p. 119.

36. J. Bardeen, L.N. Cooper, and J.R. Schrieffer, Phys. Rev. 108, 1175 (1957).

37. E.E. Havinga, Phys. Letters 26A, 244 (1968)

38. Ryusuke Hasegawa, Ph.D. Thesis, California Institute of Technology (1969).

39. A.A. Abrikosov and L.P. Gorkov, Soviet Phys. JEPT 12, 1243 (1961).

40. R.D. Parks, Superconductivity (M. Dekker, New York, 1969), p. 632.

41. David Markowitz and Leo P. Kadanoff, Phys. Rev. 131, 563 (1963).

42. G. Boato, G. Gallinaro and C. Rizzuto, Phys. Letters 5, 20 (1963).

43. Douglas L. Martin, Phys. Rev. 138, A464 (1965).

44. Wolfgang Opitz, Z. Physik. 141, 263 (1955).

45. W.B. Pearson, A Handbook of Lattice Spacings and Structures of Metals and Alloys (Pergamon Press, Inc., New York, 1957), Vol. 1; and Vol. 2

(1967).

46. H. Jones, Proc. Roy. Soc. (London) A144, 224 (1934).

47. H. Jones, Proc. Roy. Soc. (London) A147, 396 (1934).

48. H. Jones, Phil. Mag. 41, 663 (1950).

49. T.B. Massalski and H.W. King, Progr. Mater. Sci. 10, 62 (1961).

50. G.V. Raynor, Proc. Roy. Soc. (London) A174, 457 (1957).

51. W. Hume-Rothery and G. Raynor, Proc. Roy. Soc. (London) A177, 27 (1940).

52. J.B. Goodenough, Phys. Rev. 89, 282 (1953).

53. D.W. Levinson, Acta Met. 3, 294 (1955).

54. F.H. Herbstein and B.L. Averbach, Acta Met. 4, 407 (1956).

55. M. Hansen, Constitution of Binary Alloys (McGraw-Hill Book Company, Inc., New York, 1958), p. 898.

56. G. Boato, G. Gallinaro, and C. Rizzuto, Phys. Rev. 148, 353 (1966).

57. E.W. Collings and F.T. Hedgecock, Phys. Rev. 126, 1654 (1962).

58. D.L. Martin, Proc. Phys. Soc. (London) 78, 1489 (1961).

59. E.W. Collings, F.T. Hedgecock and Y. Muto, Phys. Rev. 134, A1521 (1964).

60. Y. Muto, Sci. Repts., Tohoku Univ. First Ser. 13, 1 (1961).

61. Kiyoshi Kume, J. Phys. Soc. (Japan) 23, 1226 (1967).

62. J.H. Wood, Phys. Rev. 126, 517 (1962).